Load introduction and transfer mechanism of K-type CFST circular section connections

Sha-Sha Song[1], Ju Chen[1*], Jiadaren Liu[2], Fangying Wang[3]

1. Institute of Structural Engineering, Zhejiang University, Hangzhou, Zhejiang, China
2. Department of Civil and Environmental Engineering, University of Alberta, Edmonton, Alberta, Canada
3. Department of Civil Engineering, University of Nottingham, Nottingham, United Kingdom

Abstract: This paper investigates the mechanism of load introduction and transfers for K-type concrete-filled steel tubular (CFST) circular section connections experimentally and numerically. Six K-type CFST connections were tested. Three-dimensional finite element (FE) models were then developed and validated against the test results, where the degradation and failure of the direct bond interaction were considered explicitly. The longitudinal strain distribution along the circumferential direction of chord-wall demonstrated that the non-uniform force transfer in the chord was caused by the one side load introduction through braces. The effects of the chord length, cross-sectional slenderness and interfacial interactions on the force transfer of tube-concrete interface were evaluated: 1) the chord length above the connecting region has a positive influence on the force transfer; 2) for the K-type CFST connections in this study, the material strength of concrete in the chord with non-compact and slender sections could not be fully utilised due to the insufficient force transfer; 3) the direct shear interaction dominated the force-transferring process from chord-wall to concrete for the compact section chord with reinforcing plates. Furthermore, the test and FE result confirmed that the load introduction length of the CFST chord with braces included the chord above the connecting region and the full connecting region. In addition, the equation of effective load introduction length for the CFST chord of the K-type connections was proposed.

Keywords: Concrete-filled steel tubes; Design; K-type connections; Load introduction length; Load transfer mechanisms

---

* Corresponding author. *E-mail address: cecj@zju.edu.cn (Ju Chen).*

1 Introduction

With the development of construction technologies for concrete-filled steel tubular (CFST) composite structures, concrete-filled circular hollow section (CHS) connections [1–14] have also become an indispensable part of the CFST composite structures, such as in CFST arch bridges and electric transmission towers. Sufficient data have been obtained for the mechanical behaviour and design of K-type CFST connections subjected to the brace axial force [11-14], while only a few studies focused on the mechanism of load introduction and transfer for the CFST chord of K CHS connections. For K-type CFST connections, the load is introduced to the chord through the braces at the connecting region, as shown in Fig. 1. The shear force, therefore, is transferred to the chord by direct shear interaction (bond and friction) or direct bearings (internal steel plates). In this case, the load introduction to the chord from the braces and the force transfer within the chord needs to be assessed.

Load introduction and transfer are conventionally considered to occur within the effective load introduction length, which shall not exceed a prescribed distance above and below the shear connection region, e.g., $2D$ in AISC 360-16 [15] and the minimum value of $2D$ and $L/3$ in Eurocode 4 (EC4) [16]. The values of D and L are the cross-section diameter and the length of the filled composite member, respectively. Several experimental studies [10,17-22] were conducted on concrete-filled columns with longitudinal plate connections (referred to as 'T-type CFST connection') to investigate the mechanism of load introduction and transfer from shear connections to CFST columns. These studies showed that the load introduction length was beyond the specified region [15,16], and the nominal bond stress specified in the design codes [15,16] (In AISC 360-16, the nominal bond stress is the minimum of $5300T/D^2$ and 1.4 MPa for circular CFST members, where T is the wall thickness of steel tube in mm; In EC4, the nominal bond stress is 0.55 MPa for circular CFST members) could also be conservative compared with the experimentally measured stress values. This can be attributed to that the nominal bond stress in design codes [15,16] was obtained by the push-out tests [23-31], in which the initial defects of tube and tube deformation during loading were too small to lead to additional mechanical resistance. However, for the CFST column with shear connections, the CFST column inevitably has a certain disturbance due to the horizontal load component of the braces, consequently, mechanical resistance can contribute to the interfacial interaction of the CFST column. Therefore, the shear stress in the tube-concrete interface of chord is much larger than the nominal bond strengths in design codes [15,16]. In this paper, the shear stress would not be discussed again for K-type CFST connections because the additional mechanical resistance occurs randomly during loading.

For the K-type CFST connections, the load is introduced from the brace to the chord through the welded connecting region between the chord and braces, and the shear force might be non-uniformly transferred in the chord circumferential direction due to that only one side of the chord is connected to the braces. Therefore, the load introduction length for the CFST chord of K CHS connection might be different from that of the CFST column with shear connection [10,17-22].

The authors have previously conducted a series of research on K-type CFST connections based on a project of a 370-meter electrical transmission tower [11,32]. The present study aims to evaluate the mechanism of load introduction and transfer for concrete-filled chords of K-type CFST connections. Six K-type CFST connections were tested to failure, and the finite element (FE) models were developed and validated against the corresponding test results. The longitudinal strain distributions along the circumferential direction of chord-wall at different heights were captured to study the non-uniform shear force transfer. The force transfer on the CFST chord was assessed according to the internal force allocation and contribution of chord-wall and inner concrete. The effects of the chord length, cross-sectional slenderness and interfacial interactions on the force transfer of tube-concrete interface were then discussed. In the end, the formula of effective load introduction length was proposed with a 95% confidence interval. The design approach would enable a rational and safe design of steel-encased K-type CFST connections in practical engineering.

2 Experimental investigation

2.1 Test specimens

Six K-type CFST connections were designed and tested. The configuration details of specimens are shown in Fig. 2. Both chord and brace members were fabricated from the commercially available straight seam CHS steel tubes, and only the chord members were filled with self-compacting concrete, as shown in Figs. 2(a)-(d). The fillet weld was adopted to connect the braces and chord. The brace ends and the bottom end of the chord were welded with end-plates. The weld profiles of the specimens were carried out in accordance with the AWS specification [33]. They were then checked using the ultrasonic technique. The ultrasonic test results deemed the quality of the welds acceptable. The end-plate thickness was 50 mm for the chord and 20 mm for each brace. The stiffening plates were welded to the end-plates at the tube end of the chord and braces for strengthening purposes, as shown in Fig. 2(a). It should be noted that the connecting region was defined as the region between the chord and braces.

The effects of the chord length above the connecting region L_{A} (see Fig. 2(a)) and reinforcement configuration were investigated in the test programme. The chord length above the connecting region L_{A} (hereinafter, denoted as 'upper chord length') varied between 600 mm and 900 mm, whilst the chord length below the connecting region L_{B} (hereinafter, denoted as 'lower chord length') and the chord length of connecting region L_{C} (hereinafter, denoted as 'connecting length') was kept at a constant value of 1208 mm and 584mm, respectively, for all the specimens. Noting that the upper and lower chord length were set to ensure sufficient force transfer region [15,16] and meet the installation dimensions of the loading device [11], whilst the connection length was determined based on the cross-sectional dimensions of the chord and braces and the angles between the chord and braces to keep the extension lines of axial loads of chord and braces intersect at one point. Previous research [10,20,21] has demonstrated that the reinforcing plates above the connection region can improve the load introduction efficiency in concrete-filled members. In this study, different configuration details of these reinforcing plates, i.e., zero, one, or two reinforcing plates, were used to evaluate the influence of the direct bearing on the load introduction within CFST chords. Figs. 2(e) and (f) show the configuration details of reinforcing plates for the SP and DP series. Table 1 summarizes the specimen dimension details. The definition of this specimen label will be discussed later in this section.

The test specimens were labelled based on the upper and lower chord length, and the number of reinforcing plates. For example, the labels “A600-B1208-NP(SP/DP)” define the specimens as follows:

1) The letter and the following digits of ‘A600’ and ‘B1208’ indicate that the length above and below connecting region is 600 mm and 1208 mm, respectively. The capital letters ‘A’ and ‘B’, refer to the first letter of above and below, respectively.

2) The last two letters indicate the number of reinforcing plates, where the letters ‘NP’, ‘SP’ and ‘DP’ refer to no plate, a single plate and double plates in the chord, respectively.

Tensile coupon tests [34] were conducted to obtain the material properties of the steel used in K-type CFST connections, i.e., the chord-wall, brace and reinforcing plate. The steel coupons were cut from the steel belonging to the same batch as the test specimens. The coupon dimensions conformed to the Chinese Standard GB/T 228.1-2010 [34] for the tensile testing of metals using 20 mm wide coupons. The obtained yield strength (f_y), tensile strength(f_u) and elastic modulus (E_s) of the chord wall, brace and reinforcing plate are presented in Table 2. Three 150 mm × 150 mm × 150 mm cubes were designed for the concrete compressive strength test. The tested cube concrete had the same mix proportion as the inner concrete in the chord of the K-type CFST connection. The curing condition of the cubes was consistent with that of the K-type CFST connection specimens. The compressive strength tests were conducted at 28 days after the casting of concrete. The average compressive strength (f_{cu}) of the concrete measured from three cubes is

52 MPa. The conversion equation $f_c = 0.8 f_{cu} = 41.6\text{MPa}$ was adopted to obtain the cylinder compressive strength of concrete.

2.2 Test setup

A photograph and a schematic view of the test setup are shown in Fig. 3. The fixed hinges and fixed support were connected to the ends of braces and one end of the chord, respectively, and the spherical omnidirectional loading device was used for loading [11]. As shown in Fig. 3, the extension lines of axial loads of chord and braces intersect at one point to eliminate the possible bending moment.

As shown in Figs. 3 and 4, the axial displacement of the concrete top surface was measured using displacement transducer D1. The detailed strain gauge arrangement is shown in Fig. 4. It can be seen that fifty-two longitudinal strains of chord-wall were measured using the strain gauges mounted evenly within three regions, i.e., regions above (L_A), within (L_C) and below (L_B) the connecting region in height. It should be noted that the strain gauges of D-5 and D-6 can not be mounted because the braces exists in this region and the strain gauges (B-*, C-* and $\bar{\text{B}}$-*, $\bar{\text{C}}$-*) were symmetrically distributed on both sides of the chord.

The braces were pre-loaded to 100 kN to check if all the equipment and measuring instruments work well before conducting the test. In the test, the braces were loaded by force control at an increment of 100 kN until yielding. After that, the load step was reduced to 50 kN until fracture failure. A duration of 6 minutes between two consecutive load steps was applied to ensure the stable status before the next load step. The test data of the attached strain gauges, displacement transducers, and loading cells were collected at a frequency of 1 Hz.

2.3 Experimental results and discussions

2.3.1 Failure modes and bearing capacities

As shown in Fig. 5, all the specimens failed at punching shear fracture of the chord-wall at the tensile side, and no obvious cracks were observed on the inner concrete after removing the outer chord-wall. The punching shear strength ($P_{\mathrm{u,test}}$) and corresponding axial compressive load ($N_{\mathrm{c,test}}$) of all the specimens are present in Table 1. It should be noted that the positive load, displacement and strain values refer to compressive behaviour in this paper. The corresponding axial compressive loads on the chord $N_{\mathrm{c,test}}$ can be expressed as:

$$N_{\mathrm{c,test}} = P_{\mathrm{u,test}} \left(\cos\theta_{\mathrm{t}} + \cos\theta_{\mathrm{c}} \right) \tag{1}$$

where θ_{t} and θ_{c} are the included angle between tensile brace and chord, compressive brace and chord, respectively. It can be seen that the chord length above the connecting region and the internal reinforcing plate type have a minor effect on the punching shear strength of K-type CFST connection. In addition, the axial compressive loads ($N_{\mathrm{c,test}}$) from the test results were compared with the predicted design strengths calculated according to AISC 360–16 [15] ($N_{\mathrm{u,AISC}}$) and EC4 [16] ($N_{\mathrm{u,EC4}}$), respectively, as presented in Table 3. All the test specimens failed to reach the predicted design strengths of $N_{\mathrm{u,AISC}}$ and $N_{\mathrm{u,EC4}}$, with the mean values of $N_{\mathrm{c,test}} / N_{\mathrm{u,AISC}}$ and $N_{\mathrm{c,test}} / N_{\mathrm{u,EC4}}$ being 0.96 and 0.81, respectively. This indicates that chord-wall punching shear failure precedes chord compression failure. Therefore, the force required to be transferred to the concrete shall be considered based on the axial compressive load (N_{c}) corresponding to the predicted punching shear strength (P_{u}) instead of the predicted axial compressive strength (N_{u}) in Table 3.

2.3.2 Load-displacement curves

The axial compressive load-displacement curves are compared in Fig. 6. The axial displacement was obtained from the readings of transducer D1. As shown in Fig. 6, a minor discrepancy can be identified from the load-displacement curves of each specimen with respect to the initial stiffness and axial compressive load. The influences of upper column length and reinforcing plates on the force transfer were not clearly observed based on the punching shear strength and corresponding axial load-displacement curves. Thus, the longitudinal strain distributions of the tube were then used to study the effects of the above two parameters in the following section.

2.3.3 Longitudinal strain distributions

Fig. 7 presents the longitudinal strain distributions of the chord-wall at an axial load level of about $0.95N_{\mathrm{c,test}}$, i.e., $N_{\mathrm{c}} = 3218\mathrm{kN}$, to avoid possible strain gauge failing before specimen failure. The longitudinal strain distributions of the chord-wall along the chord height were obtained from the readings of the longitudinal strain gauge. It should be noted that the longitudinal strains on positions B and C (Fig. 5) were calculated based on the average values of the strain gauges (B-* and $\bar{\mathrm{B}}$-*, C-* and $\bar{\mathrm{C}}$-*) readings at the symmetrical locations. As shown in Fig. 7, the strains of chord-wall increased significantly in the lower half of the connecting region, i.e., the height between 1200 mm and 1600 mm. The maximum strain values occurred near the lower boundary of the connecting region, indicating the occurrence of local buckling for chord-wall in this location. Furthermore, the maximum strain of chord-wall near the braces was more than that of chord-wall far away from. It can also be found that the strain values of chord-wall were nearly identical for different specimens within the chord height below the connecting region (0 ~ 1208 mm). For specimens with the same L_{A}, reinforcing plates had little influence on the strains of chord-wall, as shown in Fig. 7. This indicates the upper chord length (L_{A}) of 600 mm for the test specimen was adequate to achieve load introduction by the direct shear interaction.

3 Finite element analyses

3.1 Finite element models

3.1.1 General descriptions

The FE models were developed using ABAQUS/ Explicit 6.14 [35]. As shown in Fig. 8, only one-half of the K-type CFST connection was modelled through employing the symmetry of the tested specimens based on the solid element of C3D8R for both steel tube and inner concrete. The reinforcing rings were merged with the chord-wall. The axial tensile and compressive loads were applied on Reference Points-1 and -2 (RP-1 and RP-2) based on the local coordinates, respectively. All degrees of freedom at the bottom chord were coupled to the RP-3 of the rigid endplate. The constraints of the RP-1, -2, and -3 were set according to the real boundary conditions in the test. The element sizes around the connecting region of chord-wall were approximately 4-8 mm, and a coarse mesh setting with element sizes of 20-25 mm was adopted for the other regions. The numbers of elements in the thickness direction of the chord-wall and reinforcing plates were two.

3.1.2 Material models of concrete and steel

For the concrete compressive behaviour, the concrete damage plasticity model in ABAQUS was adopted, with default values of 0.1, 1.16 and 0.00025 assigned to parameters of flow potential eccentricity (e_{con}), the ratio of the compressive strength under biaxial loading to uniaxial compressive strength ($f_{\mathrm{bo}} / f_{\mathrm{co}}$) and viscosity parameter (μ_{v}), respectively. The other two parameters, i.e., the compressive meridian (K_{c}) and dilation angle (ψ), were determined using Eqs. (2) and (3) suggested by Tao et al. [36].

$$K_{\mathrm{c}} = \frac{5.5}{5+2(f_{\mathrm{c}})^{0.075}} \tag{2}$$

$$\psi = \begin{cases} 56.3(1-\xi) & \xi \le 0.5 \\ 6.672\mathrm{e}^{\frac{7.4}{4.64+\xi}} & \xi > 0.5 \end{cases} \tag{3}$$

where $\xi = A_{\mathrm{st}} f_{\mathrm{y,t}} / A_{\mathrm{c}} f_{\mathrm{ck}}$ is the confinement factor; $f_{\mathrm{y,t}}$ and $f_{\mathrm{ck}} = 0.67 f_{\mathrm{cu}}$ are the yield strength of chord-wall steel and characteristic cube compressive strength of concrete, respectively; A_{st} and A_{c} are the cross-sectional area of chord-wall and concrete, respectively. The elastic modulus and Poison’s ratio were taken as $E_{\mathrm{c}} = 4730\sqrt{f_{\mathrm{c}}}$ [37] and 0.2. The measured strength of concrete f_{c} was used in defining the uniaxial stress-strain relationship by the concrete constitutive model suggested by Saenz [38] (the stage before stress reaches f_c) and Han et al [39] (post-peak stage).

For the tensile behaviour of concrete, a linear relationship was adopted before reaching the tensile strength f_t, which is determined using Eq. (4) [40]. After that, the fracture energy cracking model was used to simulate the tension-softening behaviour of tensile concrete. The fracture-energy criterion was defined as Eq. (5).

$$f_t = 0.3(f_{ck})^{2/3} \tag{4}$$

$$G_F = 73(f_{ck} + 8)^{0.18}\ (\mathrm{N/m}) \tag{5}$$

For steel material, the constitutive model was defined as the von Mises yield criterion associated with the flow rule of isotropic strain hardening. For both the validation of the developed FE models and the FE-based parametric study, the stress-strain relation of steel was defined as a five-stage stress-strain model [41]. The elastic modulus, yield stress and ultimate stress were taken from tensile coupon test results, as presented in Table 2. The Poisson's ratio of steel was taken as 0.3. The modified Mohr-Coulomb criterion (MMC) model was adopted in FE simulations to predict fracture initiation and propagation [4,11,42-44].

3.1.3 Contact interaction between the steel tube and concrete

According to the specification of AISC 360-16 [15], the interaction behaviour of the tube-concrete interface includes: 1) direct bearing, i.e., mechanical resistance which is a physical interlocking mechanism, such as steel headed stud or steel channel anchors; 2) direct bond interaction, i.e., a chemical bond which is resulted from the adherence of the cement to the steel surface. In addition, the frictional resistance shall be considered in the FE models based on the guideline of ABAQUS [35] due to the mutual extrusion between the chord-wall and inner concrete. It should be noted that the direct bond interaction together with frictional resistance are considered as the direct shear interaction in this paper.

1) Direct bearing

In this study, the contribution of direct bearing caused by chord-wall initial imperfection (deformation) was not considered in the contact simulation. For K-type CFST connection without internal reinforcing plates, only the direct shear interaction (i.e., direct bond interaction and friction resistance) was involved to the force transfer. For K-type CFST connection with internal reinforcing plates, the reinforcing plates shall be considered as a contributing part to the force transfer from chord-wall to concrete. Therefore, the reinforcing plates were modelled to be embedded in the concrete to simulate the mechanical resistance in the developed FE model, whilst surface-to-surface contact behaviours, i.e., the direct bond interaction and friction resistance, were assigned to the tube-concrete interface.

2) Direct bond interaction

For the direct bond interaction simulated in the FE model, surface-based cohesive behaviour [10] provides a simplified way to model cohesive contacts with negligibly small interface thicknesses. As shown in Fig. 9, the traction-separation relationship that governs the surface-based cohesive behaviour contains: 1) linear elastic traction-separation (stage O-A); 2) damage initiation and evolution law (stage A-B). It should be noted that the damage in surface-based cohesive behaviour is an interaction property, not a material property.

In the linear elastic traction-separation stage, the normal and shear stresses (τ_n, τ_s and τ_t) to the normal and shear separations (δ_n, δ_s and δ_t) across the interface were related based on the underlying element stiffness (K_{nn}, K_{ss} and K_{tt}), as expressed in Eq. (6). All slave nodes of the tube-concrete interface were assigned with the cohesive behaviour which were assumed to be uncoupled. When the tube and concrete separated, no traction stress was generated. Therefore, the normal stiffness K_{nn} was assumed to be zero as the resistance to the surface separation is negligible [4]. The two shear stiffnesses K_{ss} and K_{tt} were determined to be 500 N/mm^3 based on the previous experimental results [10]. The quadratic stress criterion was used as the damage initiation criteria of surface-based cohesive behaviour, as expressed in Eq. (7), whilst the deterioration factor (D_{tra}) was zero. As shown in Fig. 9, the cohesive behaviour was degraded with the increase of the deterioration factor, which is defined as a linear damage evolution law based on the separation. The formulae of damage evolution law are expressed as Eqs. (8) and (9).

$$\begin{Bmatrix} \tau_{\mathrm{n}} \\ \tau_{\mathrm{s}} \\ \tau_{\mathrm{t}} \end{Bmatrix} = \begin{Bmatrix} K_{\mathrm{nn}} & 0 & 0 \\ 0 & K_{\mathrm{ss}} & 0 \\ 0 & 0 & K_{\mathrm{tt}} \end{Bmatrix} \begin{Bmatrix} \delta_{\mathrm{n}} \\ \delta_{\mathrm{s}} \\ \delta_{\mathrm{t}} \end{Bmatrix} \tag{6}$$

$$\left(\frac{\tau_{\mathrm{n}}}{\tau_{\mathrm{n}}^{\mathrm{o}}}\right)^2 + \left(\frac{\tau_{\mathrm{s}}}{\tau_{\mathrm{s}}^{\mathrm{o}}}\right)^2 + \left(\frac{\tau_{\mathrm{t}}}{\tau_{\mathrm{t}}^{\mathrm{o}}}\right)^2 = 1 \tag{7}$$

$$D_{\mathrm{tra}} = \frac{\delta_{\mathrm{m}}^{\max} - \delta_{\mathrm{m}}^{\mathrm{o}}}{\delta_{\mathrm{m}}^{\mathrm{f}} - \delta_{\mathrm{m}}^{\mathrm{o}}} = \frac{\tau_{\mathrm{m}}^{\mathrm{o}} - \tau_{\mathrm{m}}^{\min}}{\tau_{\mathrm{m}}^{\mathrm{o}}} \tag{8}$$

$$\begin{aligned} \tau_{\mathrm{n}} &= (1\text{-}D_{\mathrm{tra}})\,\bar{\tau}_{\mathrm{n}} \\ \tau_{\mathrm{s}} &= (1\text{-}D_{\mathrm{tra}})\,\bar{\tau}_{\mathrm{s}} \\ \tau_{\mathrm{t}} &= (1\text{-}D_{\mathrm{tra}})\,\bar{\tau}_{\mathrm{t}} \end{aligned} \tag{9}$$

$$\tau_{\mathrm{ini}} = 2.314 - 0.0195\frac{D_{\mathrm{c}}}{T} \tag{10}$$

where τ_{n}, τ_{s} and τ_{t} are the traction stress components in the normal and two shear directions, which are predicted by the elastic traction-separation behaviour for the current separations without damage; δ_{n}, δ_{s}, δ_{t} and K_{nn}, K_{ss}, K_{tt} are the corresponding separation and stiffness values in the same direction with τ_{n}, τ_{s} and τ_{t}, respectively; $\tau_{\mathrm{n}}^{\mathrm{o}}$, $\tau_{\mathrm{s}}^{\mathrm{o}}$ and $\tau_{\mathrm{t}}^{\mathrm{o}}$ are the traction stress components of damage initiation in the normal and two shear directions, and $\tau_{\mathrm{s}}^{\mathrm{o}} = \tau_{\mathrm{t}}^{\mathrm{o}}$ is determined using Eq. (10) in this study; $\delta_{\mathrm{m}}^{\max}$ is the maximum separation value achieved during the damage evolution process and $\tau_{\mathrm{m}}^{\min}$ is the corresponding minimum traction stress value achieved during the damage evolution process; $\delta_{\mathrm{m}}^{\mathrm{o}}$ and $\tau_{\mathrm{m}}^{\mathrm{o}}$ are the effective separation and traction stress at damage initiation, respectively; $\delta_{\mathrm{m}}^{\mathrm{f}}$ is the effective separation at bond failure; the subscript 'm' can be replaced by 'n', 's' and 't', representing the variables in corresponding directions; τ_{ini} is the bond stress between steel tube and inner concrete; $D_{\mathrm{c}}= D\text{-}2T$ is the diameter of the concrete; D is the diameter of the chord; T is the thickness of chord-wall. It should be noted that, before a surface-based cohesive behaviour was defined as general contact in ABAQUS/Explicit [35], the contact pairs and initially bonded crack surfaces (interfaces of tube-concrete) shall be established.

3) Friction resistance

The friction resistance is also part of the direct shear interaction to be used to transfer load between the chord-wall to concrete. The Coulomb friction model with a frictional coefficient (μ_{f}) of 0.6 [39] was adopted to simulate the roughness of friction behaviour, and the hard contact behaviour in the normal direction was defined to ensure strong contact pressure (P) on the interface of tube-concrete. It was assumed that only the cohesive model was active before damage initiation. Otherwise, the friction resistance ($\mu_{\mathrm{f}} P$) would contribute to the shear resistance.

3.2 Validations

The failure modes of K connections obtained from the FE simulation were compared with the test results, as shown in Fig. 5. It can be seen that the developed FE models can replicate the punching shear fracture and cracking propagation. The axial load-displacement curves of specimens obtained from the FE models and tests are compared in Fig. 10. The experimental and numerical results of strain distributions along the heights of the chord-wall are compared in Fig. 7. It should be noted that during the loading process, the strain gauge D7 was damaged due to large deformation of the chord-wall at this position. The axial compressive load of chord corresponding to the punching shear strength from the tests and FE models are compared in Table 3, with the mean value and coefficient of variation (COV) of $P_{\mathrm{u,FE}} / P_{\mathrm{u,test}}$ being 1.01 and 0.012, respectively. The comparison results demonstrate that the established FE models can accurately and reliably predict the load introduction and transfer of K-type CFST connection.

4 Typical force transfer behaviour

4.1 Non-uniform strain distributions

Longitudinal strain distributions obtained from the FE models along the circumferential direction of chord-wall are presented in Fig. 11. It can be seen that the chord-wall strain was unevenly distributed along the circumferential direction: 1) At the chord height of 168 mm, the compressive strains at the point A-0 (angle of 0°), i.e., the point far away from the braces, were approximately two times greater than that at the point A-180 (angle of 180°), i.e., the point near the braces; 2) At the chord height of 1190 mm and 1820 mm, respectively, the strains of chord-wall at the point A-0 (angle of 0°), i.e., the point far away from the braces, were much less than that at the point A-180 (angle of 180°), i.e., the point near the braces. The former was approximately one-tenth of the latter, and the strains increased significantly in the angle range of 120° to 240° (the connection region of braces and chord). The non-uniform strain distribution was more obvious as the height was closer to the connecting region. It would be attributed to 1) the stress concentration existing in this region, as discussed in the previous studies [11,45]; 2) the non-uniform force transfer in the chord caused by the one side load introduction through braces.

4.2 Force allocation

Fig. 12 presents the force distributions along the chord height with different load levels, i.e., 40%, 60%, 80% and 95% of the maximum compressive load $N_{c,FE}$. The forces of different components (chord, chord-wall and inner concrete) were obtained by the FE results of the A600-B1208-NP and A600-B1208-DP models. As shown in Figs. 12(a) and (d), the total force of chord increased gradually within the connecting region. It indicates that the load introduction through braces can be achieved for K-type CFST connections. In addition, as shown in Figs. 12(b) and (e), when the chord load reached 95% of the maximum compressive load $N_{c,FE}$, the maximum compression force in the chord-wall achieved the yield strength at the height of about 50 mm. Moreover, it can be found that the force can be transferred from chord-wall to inner concrete as shown in Figs. 12(c) and (f). This demonstrates that the force transfer from chord-wall to inner concrete can be achieved by the interfacial interactions, i.e., the direct shear interaction and direct bearing.

The load introduction and transfer within the tube-concrete interface were initiated from the chord above the connecting region, as shown in Figs. 12(b)-(c) and (e)-(f). With the increase of chord load, the bearing load in the inner concrete kept increasing until reaching the axial compression strength of concrete at the height of 1500 mm which was the intersection location of the central extension lines of the two braces. At this height of chord (1500 mm), the shearing action (as illustrated in Fig. 13) caused by the horizontal force component F_L of the compressive brace shall be considered in the local concrete resulting in the cross-sectional stress of concrete was more than that of concrete at the other height. The lateral force component also caused the localised resultant force, approximately forming an angle of about 45° with the column axis. This case was different from the T-type CFST connection. Within the height range of 1500 mm to 1200 mm, the shear action was gradually decrease due to the horizontal force component of tensile brace, which would lead to the bearing load of concrete decrease.

For the chord above the connecting region, the interfacial shear force led to that the chord-wall was in tension while the concrete was in compression, as shown in Fig. 12. The load introduction length above the connecting region was 300 mm approximately. This indicates that the upper chord length of 600 mm was long enough for the effective force transfer in each component of the K-type CFST connection. Within the connecting region, the bearing loads of chord-wall and inner concrete changed significantly and the maximum bearing load in the inner concrete was achieved in this region. This shows that the full connecting region can be considered as the effective force transfer length. For the chord underneath the connecting region, the bearing loads on the chord-wall and inner concrete were kept almost invariant. It demonstrates that the force of each component would not be transferred under the connecting region. It should be noted that the force transfer was affected by the end restraint effect (as shown in Fig. 8) near the fixed end of the chord.

For the specimen with double reinforcing plates A600-B1208-DP, the reinforcing plates have a minor impact on the force distribution of each component compared with that of the A600-B1208-NP specimen without reinforcing plates. Take the reinforcing plate at the location of SP-1 as examples, Fig. 14 (a) demonstrated that the highly concentrated stresses of reinforcing plate were found near the intersection region and plate stress of the other region were much less than the yield strength, i.e., 276.2 MPa, when the ultimate state of connections reached. This indicates that the direct shear interaction on the tube-concrete interface was the main contribution to the force transfer of the A600-B1208-DP specimen.

4.3 Strength contributions

The strength contribution from chord, chord-wall and inner concrete at different member heights, i.e., 20 mm, 1200 mm, 1500 mm, are presented in Figs. 15 and 16 by taking the specimens of A600-B1208-NP and A600-B1208-DP as examples. In Fig. 15, the strength contributions of chord-wall and inner concrete were normalized by the chord bearing load, and the strength contribution of chord (as shown in the red curve in Fig. 15) was normalized by the maximum compressive load $N_{c,FE}$ of chord, which is corresponding to the punching shear strength of the K connection. The horizontal dotted lines refer to the strength proportions of the chord, chord-wall and inner concrete in the same colours as the corresponding curves. The proportion values were calculated as the component plastic strengths, i.e., $f_{y,t}A_{st} + f_cA_c$ (chord), $f_{y,t}A_{st}$ (chord-wall) and f_cA_c (inner concrete), normalized by the total plastic strength, i.e., $f_{y,t}A_{st} + f_cA_c$, respectively. In Fig. 16, the bearing loads of chord, chord-wall and inner concrete were normalized by the corresponding component strengths, i.e., $f_{y,t}A_{st} + f_cA_c$ (chord), $f_{y,t}A_{st}$ (chord-wall) and f_cA_c (inner concrete).

As shown in Figs. 15(a) and (b), at the height of 1500 mm, the bearing load was mainly contributed from the inner concrete where the load proportions were much higher than the plastic strength proportions, and the material strength of inner concrete was almost fully utilized at this height, as presented in Figs. 16(a) and (b). This indicates that the shear force can be efficiently transferred from the chord-wall to inner concrete. At the height of 1200 mm, the strength contributions of chord-wall and inner concrete were about 50% and were both close to the corresponding plastic strength proportions, whilst the utilization rates of material strengths of chord-wall and inner concrete could reach 90% and 85%, respectively, at the ultimate stage of connection, as shown in Figs. 15(c)-(d) and Figs. 16(c)-(d). This demonstrates that most of the material strengths for each component can be utilized below the connecting region. At the height of 20 mm, a minor increase of the chord-wall and reduction of the inner concrete strengths can be found in Figs. 15(e)-(f) and Figs. 16(e)-(f). This indicates that further force transfer within each component would occur near the end of chord, which was caused by the restraint effect of fixed support at this position.

From the comparison of the A600-B1208-NP and -A600-B1208-DP specimens, the reinforcing plates have a minor impact on the force transfer mechanism. Generally, both NP and DP specimens can develop the effective utilization rates of material strengths for each component when the K connections fail at punching shear fracture. It should be noted that when the K connections reached the plastic yield stage, the curves of chord-wall and inner concrete in Fig. 16 exhibited minor fluctuations caused by a small amount of the shear force transferred between the chord-wall and inner concrete.

5 Parametric analyses

The developed FE models were used for parametric analyses to further investigate the mechanisms of load introduction and transfer. The considered parameters include the upper and lower chord lengths, the cross-sectional slenderness of chord and the interfacial interactions. The label of the parametric FE models is defined based on the outer diameter and thickness of chord wall, upper and lower chord length, and the number of reinforcing plates. The angle between the chord and brace in FE models is consistent with that of the specimens. Therefore, the connection lengths (L_C) were 584 and 614 mm for D273T8 and D300T8 series, respectively. For comparison purposes, the properties of the inner concrete, chord-wall and brace are the same as the test material. The loading and boundary conditions in the models for parametric studies are identical to the validated FE models in Section 3.

5.1 Effect of upper and lower chord lengths, L_A and L_B

The effect of CFST chord lengths above and below the connection region on the mechanism of load introduction and transfer had been evaluated by previous studies [10,17,20,21]. Dunberry et al [17] showed that the introduction length extended for a distance of 3*D* to 3.5*D* below and *D* to 2*D* above the connection, which is the basis of current design methods [15,16]. Differently, Mollazadeh et al and Xu et al [10,20,21] showed that only the lengths above and within the connection region were active in load introduction. Therefore, to assess the influence of the upper and lower chord lengths on the mechanism of load introduction and transfer, five K-type CFST connections with the D273T8 series chord ($L_{\mathrm{A}} = 0,\ 300,\ 600,\ 900,$ and $1200\ \mathrm{mm}$, $L_{\mathrm{C}} = 584\ \mathrm{mm}$, $L_{\mathrm{B}} = 1208\ \mathrm{mm}$) and four connections with the D300T8 series chord ($L_{\mathrm{B}} = 600,\ 900,\ 1208$ and $1500\ \mathrm{mm}$, $L_{\mathrm{A}} = 600\ \mathrm{mm}$, $L_{\mathrm{C}} = 614\ \mathrm{mm}$) were simulated numerically in this section.

A comparison of load-axial strain curves with different parameters is presented in Fig. 17. As shown in Fig. 17(a), a slight increase in maximum compressive load ($N_{\mathrm{c,FE}}$) of the chord can be observed with the increase of upper chord length (L_{A}). Furthermore, the comparison results (in terms of strength utilization and contribution of each component) of the FE models with the same lower column length but different upper column lengths varying as 0, 300, 600, 900 and 1200 mm are present in Fig. 18. It can be seen that the increase of the upper chord length (L_{A}) could increase the strength contribution of inner concrete, whilst decrease the strength contribution of chord-wall. This demonstrates that the load introduction efficiency can be improved by increasing the length of upper chord (L_{A}), resulting in more shear force that can be transferred from the chord-wall to inner concrete. Moreover, the increase in upper chord length can improve the external load allocation (strength allocation scheme) ability in the chord. The numerical and experimental results confirm that the load introduction length can be increased by increasing the upper chord length (L_{A}). On the contrary, as shown in Fig. 17(b), the lower chord length (L_{B}) had a negligible effect on the maximum compressive load of the chord, which indicates that the load introduction and transfer were not critical below the connecting region.

5.2 Effect of cross-sectional slenderness

According to the specification of AISC 360–16 [15], the sections of compressive concrete-filled members can be classified as compact, non-compact and slender based on the value of width-to-thickness ratio (D/T). The CFST chord of K CHS connections with a chord-wall diameter (D) of 273 mm and thicknesses (T) of 8, 4, 2, and 1.6 mm were classified as compact, compact, non-compact and slender members, respectively. As shown in Fig. 17(c), the compressive load ($N_{c,FE}$) of chord corresponding to the punching shear strength increased with the increase of chord-wall thicknesses. It may be attributed to that the ultimate compressive load of chord is a vertical component of the punching shear strength ($P_{u,FE}$) (as expressed in Eq. (1)), and Song et al [11] showed that the punching shear strength of K-type CFST connections was positively correlated with the chord-wall thicknesses. On the other hand, the chord-wall confinement effect increases with the decrease of the width-to-thickness ratio, which improves the ability of the load introduction and force transfer of the CFST chord, resulting in the increased compressive load of the chord.

The strength utilization and contribution curves of each component are present in Fig. 19. The chords with non-compact and slender sections, i.e., D273T2 and D273T1.7 series had similar strength utilization and contribution curves, and their strength utilization of inner concrete was less than 50% because of insufficient load transfer. Meanwhile, when the punching shear strength reached, it can be seen from Figs. 19(d) and (e) that compared with the the non-compact and slender section chords of D273T2 and D273T1.7 series, the bearing load proportions of chord-wall and inner concrete of the compact section chord of D273T8 series were closer to the corresponding plastic strength proportions. The numerical results indicate that the load introduction and transfer are insufficient for the non-compact and slender chords of K-type CFST connections in this study. For compact chords, with the decrease of width-to-thickness ratio, the material utilization ratio of each component and the load introduction length in the upper chord increased, as shown in Figs.

19(a)-(c) and 20. This can be attributed to the improved ability of confinement provided by the tube.

5.3 Effect of interfacial interactions

As mentioned in Section 5.1, the upper chord length (the direct shear interaction) had a positive but not significant effect on the force transfer of tube-concrete interface, and Xu et al [10] showed that the direct bearing, i.e., reinforcing plates, could effectively improve the force transfer ability for steel-encased CFST columns of T-type CFST connections. Therefore, the direct bearing should be considered to improve the ability of force transfer for the CFST chord of K CHS connection.

For concrete-filled members, the external force is transferred into the inner concrete by the direct bearing from reinforcing plates and the direct shear interaction. The largest nominal strength of the two interfacial interactions (direct bearing and direct shear interaction) will be provided for the shear transfer within the tube-concrete interface. In this section, the reinforcing plates [10] were used as the direct bearing in the CFST chords of the K CHS connections, such as the test specimens in the SP and DP series. It should be noted that to consider the position influence, three FE models with one reinforcing plate located at 10 mm (SP-1) and 300 mm (SP-2) above and 10 mm below (SP-3) the connecting region were established for the SP series. To assess the effects of interfacial interactions (direct bearing and direct shear interaction) on the force transfer mechanism for K-type CFST connections, D300T8A600B1208 and D300T8A900B1208 series were selected. It should be noted that the upper length of 600 mm is sufficient to achieve the maximum effect of the direct shear interaction. The configuration details of reinforcing plates for the SP and DP series are shown in Fig. 2(e) and (f). The width of the reinforcing ring plates (w_p) was calculated according to Eq. (11).

$$V_{\mathrm{in,bearing}} = 1.7 f_c \frac{\left[\left(D_1\right)^2 - (D_1 - 2w_p)^2\right]\pi}{4} = N_{\mathrm{c(NP)}}\left(1 - \frac{f_{y,t}A_{st}}{N_{\mathrm{no,AISC}}}\right) \tag{11}$$

where $V_{\mathrm{in,bearing}}$ is the available bearing strength of the concrete for the limited state of concrete crushing, and it should meet the requirement of the shear force to be sufficiently transferred from chord-wall to the inner concrete by the reinforcing plates [15]. D_1 is the diameter of reinforcing ring plate; $N_{c(NP)}$ is the vertical force component of predicted punching shear load [11] (P_u) of the corresponding K connections in NP series, i.e., D300T8A600B1208NP and D300T8A900B1208NP. $N_{no,AISC}$ is the nominal axial compressive strength of the corresponding CFST chord without consideration of length effects and can be calculated according to AISC 360-16. The plate thickness is the same as the test specimens, i.e., 6 mm.

The load-strain curves with different numbers and positions of reinforcing plates are presented in Figs. 17(d) and (e). A negligible discrepancy was observed in the load-strain curves of CFST chords with different numbers and positions of reinforcing plates. This demonstrates that the interfacial interactions, i.e., the direct bearing and direct shear interaction, can not be superimposed, and the direct shear interaction dominated the force transfer before the initiation of direct bearing. It may be attributed to the fact that the vertical component of punching shear load for K-type CFST connections was insufficient to cause relative sliding between the chord-wall and inner concrete. The stress distribution of reinforcing plate at the location of SP-1 for the D300T8A600B1208DP specimen is presented in Fig. 14(b). The stresses of reinforcing plate were far below the yield strength when the ultimate state of connections was reached. Furthermore, the plying force could be found in the region away from the connection region, as illustrated in Fig. 21, although the local compression was actively localised in the connecting region. Therefore, the stress distribution and plying force of reinforcing plates above the connecting region indicate the reason for the little contribution of the direct bearing from the reinforcing plates to load transfer. The direct bearing, therefore, was not involved in the force transfer process. The numerical results confirm that for the CFST chord of K connections, the direct shear interaction is sufficient for load transfer from chord-wall to concrete, and the external load allocation in the chord-wall and inner concrete is ideal, as shown in Fig. 22. It should be noted that the plate below the connecting region (SP-3 series) for the

CFST chord of K connection would result in stress concentration right below the connection region, which triggered a local buckling of the tube, as indicated in Fig. 23.

6 Load introduction length

The comparison results from the parametric study demonstrate that the non-compact and slender sections should not be used in the CFST chord with braces because of inadequate load transfer. Therefore, the non-compact and slender section chords would not be studied in this section. On the other hand, the direct shear interaction is sufficient for the load transfer from chord-wall to inner concrete for K-type CFST connections, and both the upper chord length and confinement effect contribute to the process of load introduction and transfer. Generally, these critical parameters shall be considered in the design method.

For K-type CFST connections with punching shear failure, typical distributions of the normalized strength of chord-wall with different width-to-thickness ratios are present in Fig. 24. It can be seen that the load introduction was initiated at a location above the connecting region. Meanwhile, the load introduction length varied with different cross-sectional slenderness. According to AISC 360–16 [15], load introduction length shall not exceed a distance of two times the diameter of a round steel member, i.e., 2D, both above and below the force transfer region for filled composite members. In this paper, for the chord above the connecting region, the introduction length in AISC 360–16, i.e., 2D, was conservatively overestimated, and the observed introduction length above the connecting region was slightly larger than the chord-wall diameter D (i.e., less than the 2D in AISC 360–16). It should be noted that the starting point of the introduction length above the connecting region was defined when the normalized strength reached 1%. The tangent at the start point was used to determine the location of starting point, as shown in Fig. 24. For the connecting region of chord, the full length of connecting region (L_C) shall be considered as the load introduction because that the chord-wall bearing loads changed significantly. For the chord underneath the connecting region, the load introduction length can be neglected, as mentioned in Section 5.1.

Generally, the load introduction length of the CFST chord with braces should include two parts: 1) the load introduction length above the connecting region, i.e., $L_{\mathrm{in,A}}$; 2) the full length of connecting region, i.e., L_{C} . The relationship between introduction lengths $L_{\mathrm{in,A}}$ above the connecting region and the parameter $\eta_{\mathrm{T\_C}}$ (in Eq. (14)) is shown in Fig. 25. The best-fitting curve of a power relationship with a 95% prediction band is presented in Fig. 25 and expressed in Eq. (15). The parameter $\eta_{\mathrm{T\_C}}$ reflects the ability of the chord-wall to provide lateral constrain on the specific interfacial perimeter $C_{\mathrm{T\_C}} / D$.

$$\eta_{\mathrm{T\_C}} = \left(\frac{D}{T}\right)\left(\frac{D}{C_{\mathrm{T\_C}}}\right)\frac{E_{\mathrm{s,t}}\left(\mathrm{GPa}\right)}{f_{\mathrm{y,t}}\left(\mathrm{MPa}\right)} \tag{14}$$

$$L_{\mathrm{in,A}} = \begin{cases} 2.84D\left(\eta_{\mathrm{T\_C}}\right)^{-0.336} & (L_{\mathrm{A}} > D) \\ L_{\mathrm{A}} & (L_{\mathrm{A}} \le D) \end{cases} \tag{15}$$

where $C_{\mathrm{T\_C}}$ is the circumference of inner concrete section. The design recommendation and the proposed equation in this section are validated for compact section chords where the range of the width-to-thickness ratio (D/T) is 25.0 to 68.3. It should be noted that the analyzed load introduction and transfer mechanism and proposed introduction length were derived based on the connection configuration in this study. In addition, the specimens were designed based on the author's previous research results on the mechanical behaviours of corresponding members [2,10,11,45], in which the potential internal defects caused by size effects of the steel-encased CFST specimens, i.e., concrete cracks, weld quality of steel, and disengaging at the tube-concrete interface, exhibit minor influence on the mechanical behaviours.

7 Conclusions

This paper experimentally and numerically investigated the mechanism of load introduction and transfer for K-type CFST connections. The interfacial behaviour on the tube-concrete interface was assessed, based on which, the effective load introduction length and interfacial shear stress for the K-type CFST connection were proposed. The following conclusions can be made in this paper:

(1) All the test specimens failed at the chord-wall punching shear fracture, meanwhile no obvious cracks were observed on the inner concrete. The upper chord length of 600 mm for the test specimens was adequate to achieve the load introduction by the direct shear interaction.

(2) The developed FE models were validated against the test results and were capable of accurately simulating the degradation and failure of the direct bond interaction for the steel-concrete interface. Based on the developed FE models, the behaviours of load introduction and transfers of concrete-filled K connection were analysed.

(3) The longitudinal strain distributions along the circumferential direction of chord-wall demonstrated that the non-uniform force transfer in the chord was caused by the one side load introduction through braces.

(4) The influence of the chord length, cross-section slenderness and interfacial interactions on the force transfer of tube-concrete interface was assessed in the parametric study. It is recommended that i) the chord length above the connecting region has a positive influence on the force transfer; ii) the ability of force transfer can be improved by increasing the width-to-thickness ratio of chord; iii) the material strength of concrete in the chord with non-compact and slender sections could not be fully utilised due to insufficient force transfer for connections in this study; iv) the direct shear interaction dominated the load transfer before the initiation of direct bearing, and the former was sufficient to enable the external load to be transferred from chord-wall to concrete for compact section.

(5) The load introduction occurred on the chord above and within the connecting region. The full connecting region shall be considered as a part of the load introduction length. In addition, the effective length of load introduction above the connecting region was proposed.

Acknowledgements

The research work described in this paper was supported by a grant from the National Natural Science Foundation of China (52078249).

References

[1] Cheng CT, Chung LL. Seismic performance of steel beams to concrete-filled steel tubular column connections. Journal of Constructional Steel Research, 2003, 59(3):405-426.

[2] Xu F, Chen J, Jin WL. Experimental investigation and design of concrete-filled steel tubular CHS connections. Journal of Structural Engineering, 2015, 141(2):04014106.

[3] Tong LW, Xu GW, Yang DL, Mashiri FR, Zhao XL. Fatigue behavior and design of welded tubular T-joints with CHS brace and concrete-filled chord. Thin-Walled Structures, 2017, 120:180-190.

[4] Xu F, Chen J, Chan TM. Numerical analysis and punching shear fracture based design of longitudinal plate to concrete-filled CHS connections. Construction and Building Materials. 2017, 156:91-106.

[5] Hou C, Han LH, Mu TM. Behaviour of CFDST chord to CHS brace composite K-joints: Experiments. Journal of Constructional Steel Research. 2017, 135:97-109.

[6] Hou C, Han LH. Analytical behaviour of CFDST chord to CHS brace composite K-joints. Journal of Constructional Steel Research. 2017, 128:618-632.

[7] Jin DYD, Hou C, Shen LM, Han LH. Numerical investigation of demountable CFST K-joints using blind bolts. Journal of Constructional Steel Research, 2019, 160:428-443.

[8] Xu F, Chen J, Guo Y, Ye Y. Innovative design of the world's tallest electrical transmission towers. Civil Engineering, 2019, 172(5):1-34.

[9] Yang YL, Liu XG, Zhang J, Liu JP, Cheng W. Behavior of large-scale connections between circular concrete-filled steel tubular columns and H-section steel beams. Advances in Structural Engineering, 2020, 23(2):307-319.

[10] Xu F, Song SS, Lai ZC, Chen J. Mechanism of load introduction and transfer within steel-encased CFST members with shear connections. Engineering structures. 2021, 242:112576.

[11] Song SS, Chen J, Xu F. Mechanical behaviour and design of concrete-filled K and KK CHS connections. Journal of Constructional Steel Research, 2022, 188:107000.

[12] Udomworarat P, Miki C, Ichikawa A, Sasaki E, Hasaka T. Fatigue and ultimate strengths of concrete filled tubular K-joints on truss girder, Journal of Structural Engineering, 2000, 46 (3):1627–1635.

[13] Sakai Y, Hosaka T, Isoe A, Ichikawa A, Mitsuki K. Experiments on concrete filled and reinforced tubular K-joints of truss girder. Journal of Constructional Steel Research, 2004, 60(3/5):683-699.

[14] Huang WJ, Fen LG, Chen BC, Briseghella B. Experimental study on K-joints of concrete-filled

steel tubular truss structures. Journal of Constructional Steel Research, 2015, 107:182-193.
[15] ANSI/AISC 360-16, Specification for structural steel buildings, America Institute of Steel Construction (AISC), Chicago, USA, 2016.
[16] CEN (European Committee for Standardization). Eurocode 4: Design of composite steel and concrete structures—Part 1-1: General rules and rules for buildings. EN 1994-1-1, London; 2004.
[17] Dunberry E, Leblanc D, Redwood RG. Cross-section strength of concrete-filled HSS columns at simple beam connections. Canadian Journal of Civil Engineering. 1987, 14(3):408–17.
[18] Jacobs WP, Hajjar JF. Load transfer in composite construction. Structures Congress 2010, ASCE, Reston, VA, 1229–1240.
[19] Johansson M. Composite action in connection regions of concrete-filled steel tube columns. Steel Composite Structures. 2003;3(1):47–64.
[20] Mollazadeh MH, Wang YC. New insights into the mechanism of load introduction into concrete-filled steel tubular column through shear connection. Engineering structures, 2014;75:139–51.
[21] Mollazadeh MH, Wang YC. New mechanism of load introduction into concrete-filled steel tubular columns. Journal of Structural Engineering, 2016, 142(6):04016016.
[22] Mollazadeh MH, Wang YC. Design implications of a new load introduction mechanism into concrete-filled steel tubular columns. Structures 2016;6:37–47.
[23] Wium JA, Lebet JP. Simplified calculation method for force transfer in composite columns. Journal of Structural Engineering, 1994, 120(3):728–746.
[24] Shakir-Khalil H. Pushout strength of concrete-filled steel hollow section tubes. Engineering structures, 1993, 71(13):230–243.
[25] Roeder CW, Cameron B, Brown CB. Composite action in concrete filled tubes. Journal of Structural Engineering, 1999, 125(5):477–484.
[26] De Nardin S, El Debs ALHC. Shear transfer mechanisms in composite columns: an experimental study. Steel Composite Structures, 2007, 7(5):377–390.
[27] Qu XS, Chen ZH, Nethercot DA, Gardner L, Theofanous M. Load-reversed push-out tests on rectangular CFST columns. Journal of Constructional Steel Research. 2013, 81:35-43.
[28] Chen LH, Dai JX, Jin QL, Chen LF, Liu XL. Refining bond-slip constitutive relationship between checkered steel tube and concrete. Construction & Building Materials. 2015, 79:153-164.
[29] Tao Z, Song TY, Uy B, Han LH. Bond behavior in concrete-filled steel tubes. Journal of Constructional Steel Research. 2016, 120:81–93.

[30] Cao JX, Liu YY, Wang YX, Zhang YM. Load-slip performance of timber-to-concrete connections with U-steel connectors under push-out test. Journal of Building Engineering. 2022, 45:103527.

[31] Li W, Chen B, Han LH, Packer JA. Pushout tests for concrete-filled double skin steel tubes after exposure to fire. Thin-walled structures. 2022, 176:109274.

[32] Xu F, Chen J, Jin WL. Experimental investigation of thin-walled concrete-filled steel tube columns with reinforced lattice angle. Thin-walled structures. 2014, 84:59-67.

[33] ANSI/AWS D1.1-96. Structural welding code-steel. American Welding Society (AWS), Miami,1996.

[34] Metallic materials tensile test part 1: Room temperature test method: GB/T 228.1—2010. Beijing: China National Standardization Administration, 2010. (in Chinese)

[35] Hibbitt HD, Karlsson BI, Sorensen P, ABAQUS Documentation Collection. Ver.6.10, USA, 2010.

[36] Tao Z, Wang ZB, Yu Q. Finite element modelling of concrete-filled steel stub columns under axial compression. Journal of Constructional Steel Research, 2013, 89(oct.):121-131.

[37] ACI 318, Building Code Requirements for Reinforced Concrete and Commentary, American Concrete Institute (ACI), Farmington Hill, Detroit, USA, 2011.

[38] Saenz LP. Discussion of “equation for the stress-strain curve of concrete” by Desayi and Krishnan. Journal of the American Concrete Institute, 1964, 61(3):345-350.

[39] Han LH, Yao GH, Tao Z. Performance of concrete-filled thin-walled steel tubes under pure torsion. Thin-walled structures. 2007, 45(1):24–36.

[40] CEB-FIP Model Code 2010, Fib model code for concrete structures 2010, federation internationale du be´ton (fib), Lausanne, Switzerland, 2012.

[41] Han LH, Concrete-filled steel tubular structures-theory and practice (Second Version), China Science Press, 2007 (in Chinese).

[42] Xu F, Chen J, Chan TM. Mechanical behaviour of concrete-filled CHS connections subjected to in-plane bending. Engineering structures. 2017, 148:101-12.

[43] Xu F, Chen J, Shu K, Su MN. Cyclic behaviour of double-tube buckling-restrained braces for boiler steel plant structures. Journal of constructional steel research. 2018, 150:556-569.

[44] Xu F, Chan TM, Sheehan T, Gardner L. Prediction of ductile fracture for circular hollow section bracing members under extremely low cycle fatigue. Engineering structures. 2020, 214:110579.

[45] Xu F, Chen J, Jin WL. Experimental investigation of SCF distribution for thin-walled concrete-filled CHS joints under axial tension loading. Thin-walled structures. 2015, 93:149-57.

Notation

The following symbols are used in this paper:

Latin upper case letters

A_c = the sectional area of inner concrete;

A_{st} = the sectional area of chord-wall;

C_{T_C} = the circumference of inner concrete section;

D = the outer diameter of the chord member;

D_1 = the diameter of reinforcing ring plate;

D_c = the diameter of the inner concrete;

D_{tra} = the bonding deterioration factor;

E_c = the elastic modulus of concrete;

E_s = the elastic modulus of coupon steel;

$E_{s,t}$ = the elastic modulus of chord-wall;

G_F = the fracture-energy-based cracking criterion;

K_c = the ratio of the second stress invariant on the tensile meridian to that on the compressive meridian;

K_{nn} = the stiffness value in the normal direction;

K_{ss} = the stiffness value in the orthogonal direction;

K_{tt} = the stiffness value in the orthogonal direction and perpendicular to the direction of K_{ss};

L = the length of the chord member;

L_A = the chord length above the connecting region;

L_B = the chord length below the connecting region;

L_C = the length of the connection region;

$L_{in,A}$ = the load introduction lengths above the connection on the tube-concrete interface;

N_c = the axial compressive loads of CFST chord corresponding to the punching shear strength of K-type CFST connection;

$N_{c,test}$ = the axial compressive loads of CFST chord corresponding to the punching shear strength of K-type CFST connection from the test result;

$N_{c,FE}$ = the axial compressive loads of CFST chord corresponding to the punching shear strength of K-type CFST connection from the FE result;

$N_{c(NP)}$ = the axial compressive loads of CFST chord corresponding to the predicted punching shear strength of K-type CFST connection in NP series;

$N_{no,AISC}$ = the nominal axial compressive strength of corresponding CFST members without consideration of length effects calculated according to AISC 360-16;

N_u = the axial compressive strength;

$N_{u,AISC}$ = the axial compressive strength according to AISC 360-16;

$N_{u,EC4}$ = the axial compressive strength according to EC4;

P = the contact pressure between steel tube and inner concrete;

P_u = the punching shear strength of K-type CFST connection;

$P_{u,FE}$ = the punching shear strength of K-type CFST connection from the FE result;

$P_{u,test}$ = the punching shear strength of K-type CFST connection from the test result;

T = the thickness of chord-wall;

$V_{in,bearing}$ = the available bearing strength of the concrete for the limited state of concrete crushing;

Latin lower case letters

d = the diameter of the brace;

e_{con} = the flow potential eccentricity;

f_{bo} = the compressive strength under biaxial loading;

f_c = the cylinder compressive strength of the concrete;

f_{ck} = the characteristic compressive strength of concrete;

f_{co} = the compressive strength under uniaxial loading;

f_{cu} = the cubic compressive strength of the concrete;

f_y = the yield strength of coupon steel;

$f_{y,t}$ = the yield strength of chord-wall;

f_t = the tensile strength of concrete;

f_u = the tensile strength of coupon steel;

l_b = the length of brace;

t = the thickness of brace;

w_p =the width of the reinforcing ring plates.

Greek case letters

θ_c = the included angle between the compressive brace and chord;

θ_t = the included angle between the tensile brace and chord;

δ_m^f = the effective separations at bond failure;

δ_m^{max} = the maximum separation value achieved during the damage evolution process;

δ_m^o = the effective separation at damage initiation;

δ_n = the traction separation in the normal direction;

δ_s = the traction separation in the orthogonal direction;

δ_t = the traction separation in the orthogonal direction and perpendicular to the direction of δ_s;

ψ = the dilation angle;

ξ $=\dfrac{A_{st} f_{y,t}}{A_c f_{ck}}$, the confinement factor;

η_{T_C} $= \left(\dfrac{D}{T}\right)\left(\dfrac{D}{C_{T\_C}}\right)\dfrac{E_{s,t}(\mathrm{GPa})}{f_{y,t}(\mathrm{MPa})}$;

μ_f = 0.6 the frictional coefficient between steel tube and inner concrete;

μ_v = the viscosity parameter;

τ_{ini} = the damage initiation traction stress;

τ_m^o = the effective traction stress at damage initiation;

τ_m^{min} = the minimum traction stress value achieved during the damage evolution process;

τ_n = the traction stress in the normal direction;

τ_n^o = the damage initiation traction stress in the normal direction;

τ_s = the traction stress in the orthogonal direction;

τ_s^o = the damage initiation traction stress in the orthogonal direction;

τ_t = the traction stress in the orthogonal direction and perpendicular to the direction of τ_s;

τ_t^o = the damage initiation traction stress in the orthogonal direction and perpendicular to the direction of τ_s^o.

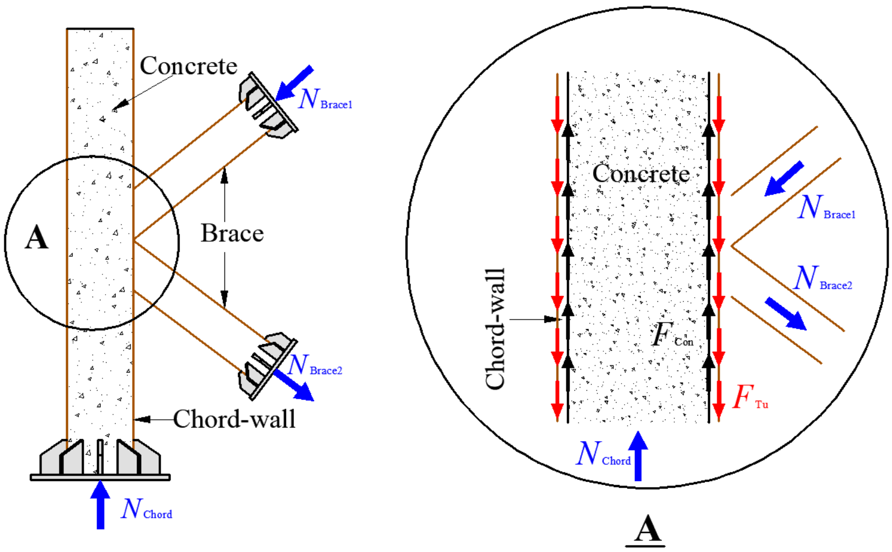

Figure 1. Load introduction and transfer mechanism

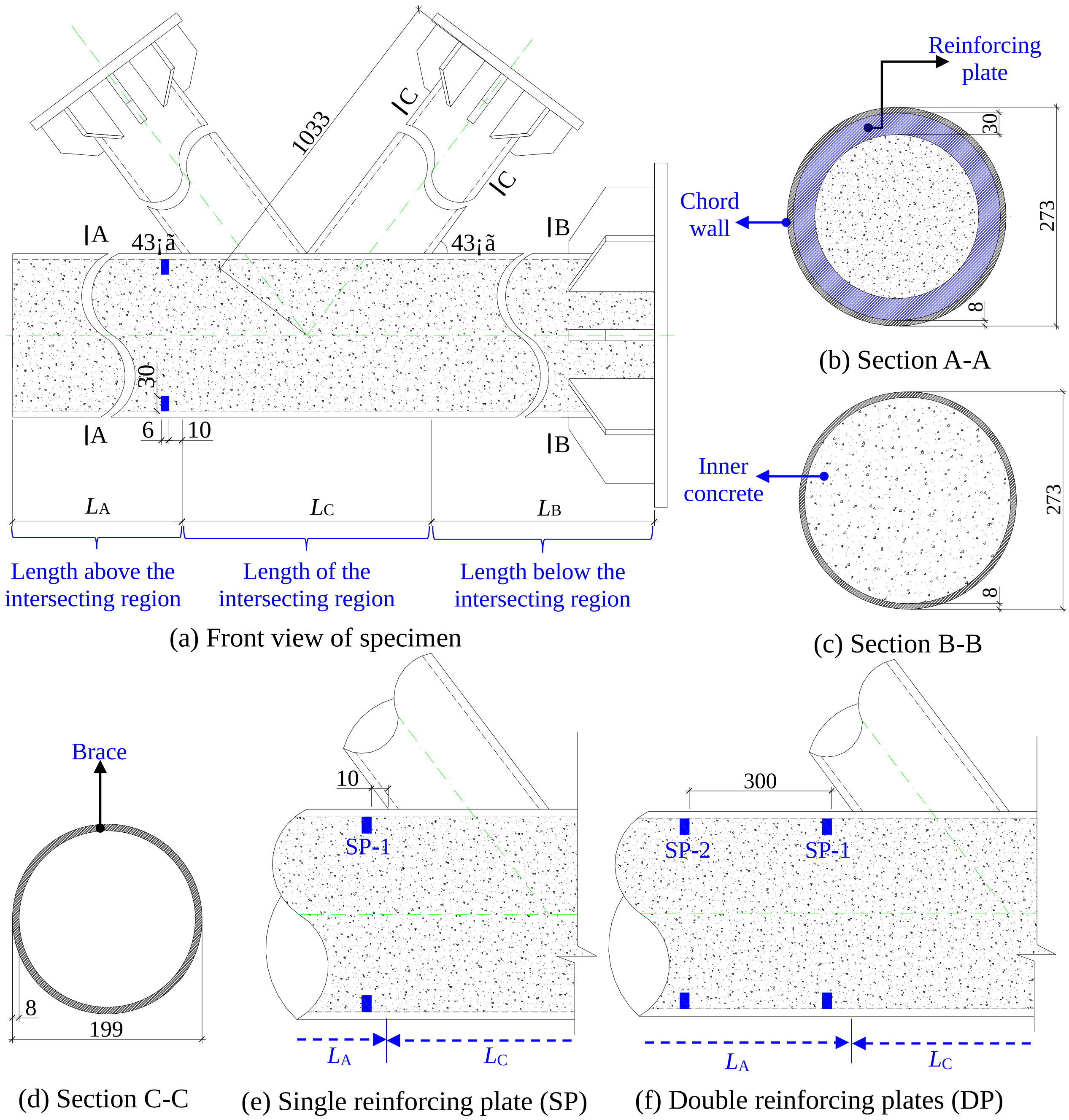

Figure 2. Dimension of test specimens (unit: mm)

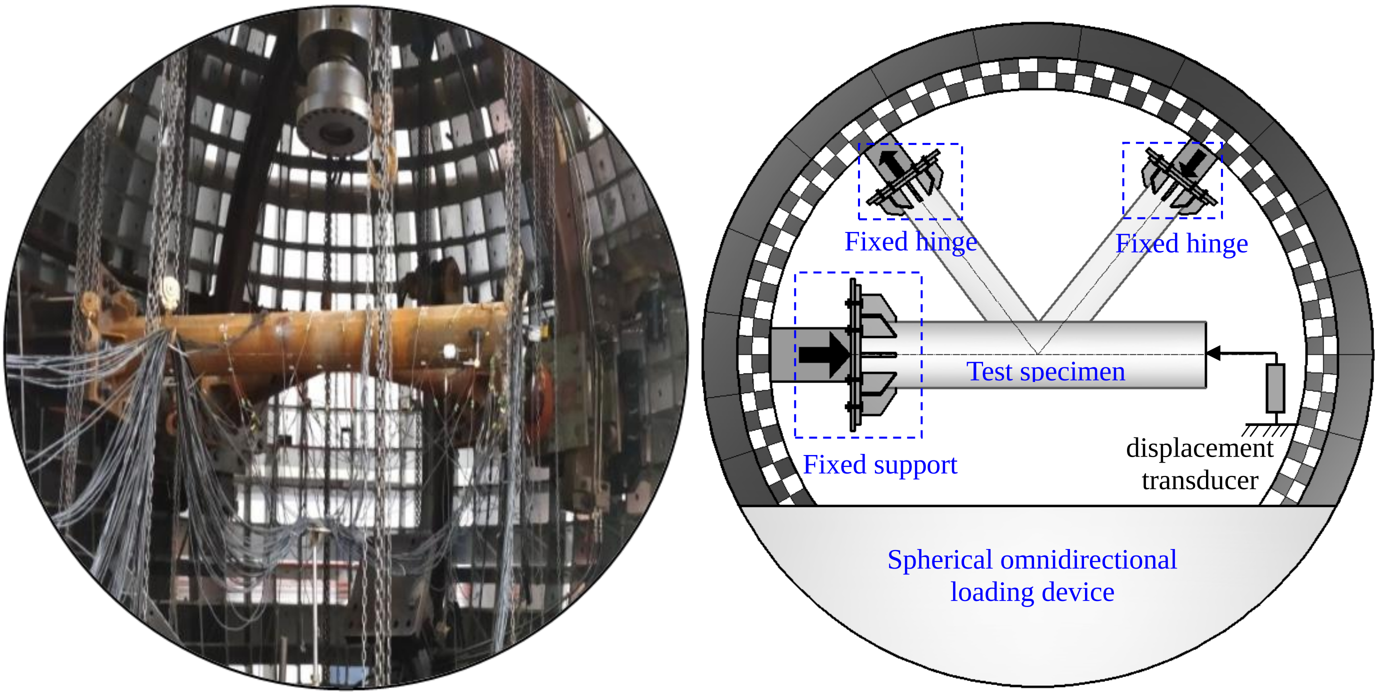

Figure 3. Test setup

(a) Photo of test specimen

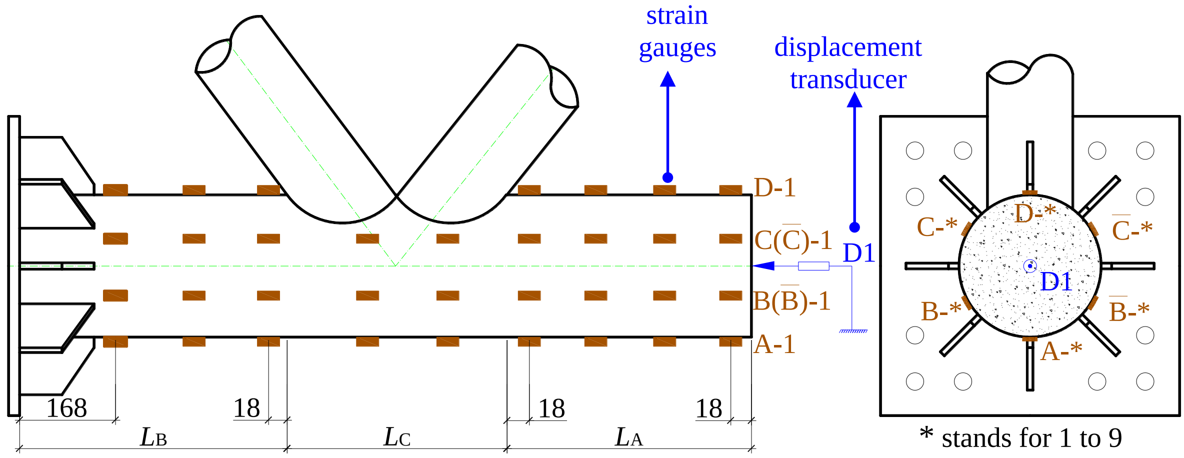

(b) Schematic diagram of the test setup

Figure 4. Arrangements of the displacement transducers and strain gauges

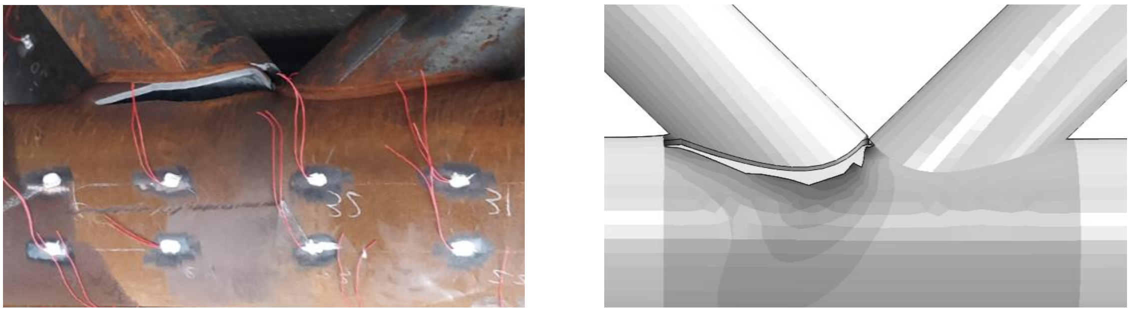

(a) Punching shear failure of chord

(b) Inner concrete

Figure 5. Failure modes of A600-B1208-NP

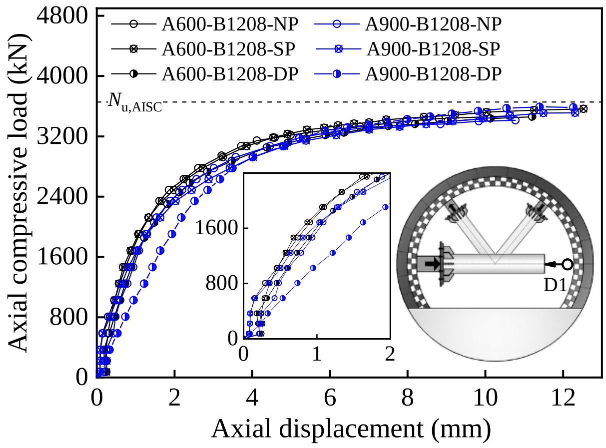

Figure 6. Axial compressive load-displacement curves of test specimens

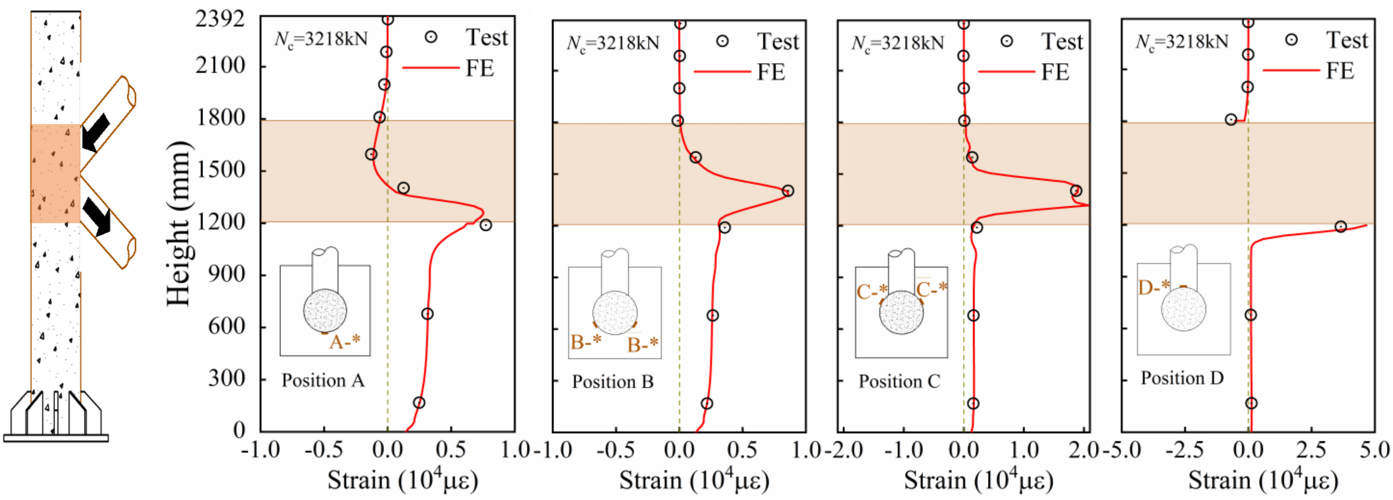

(a) A600-B1208-NP

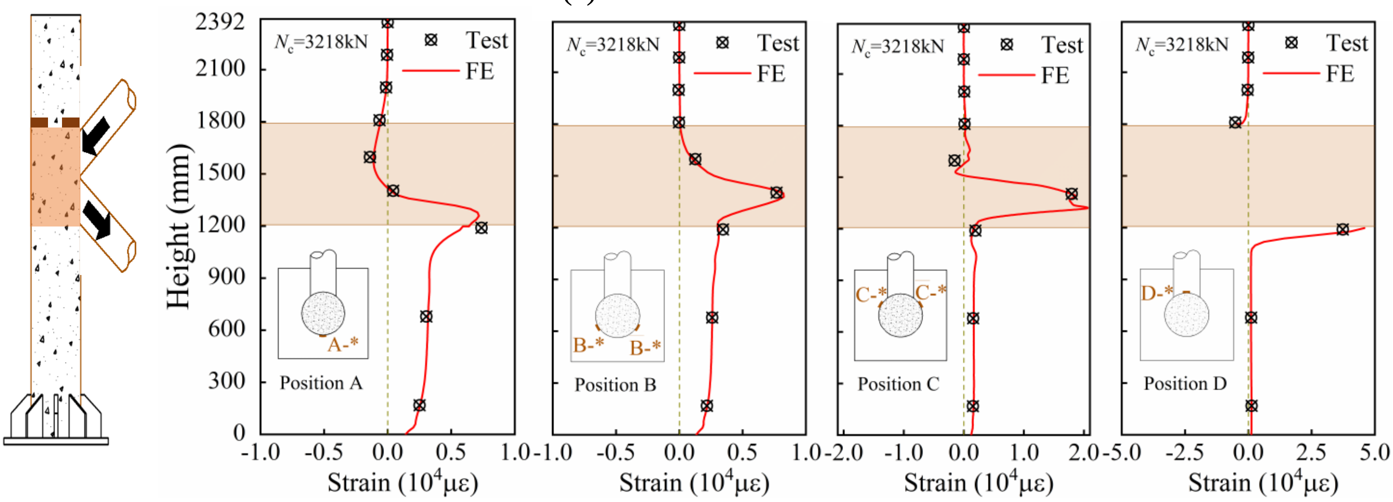

(b) A600-B1208-SP

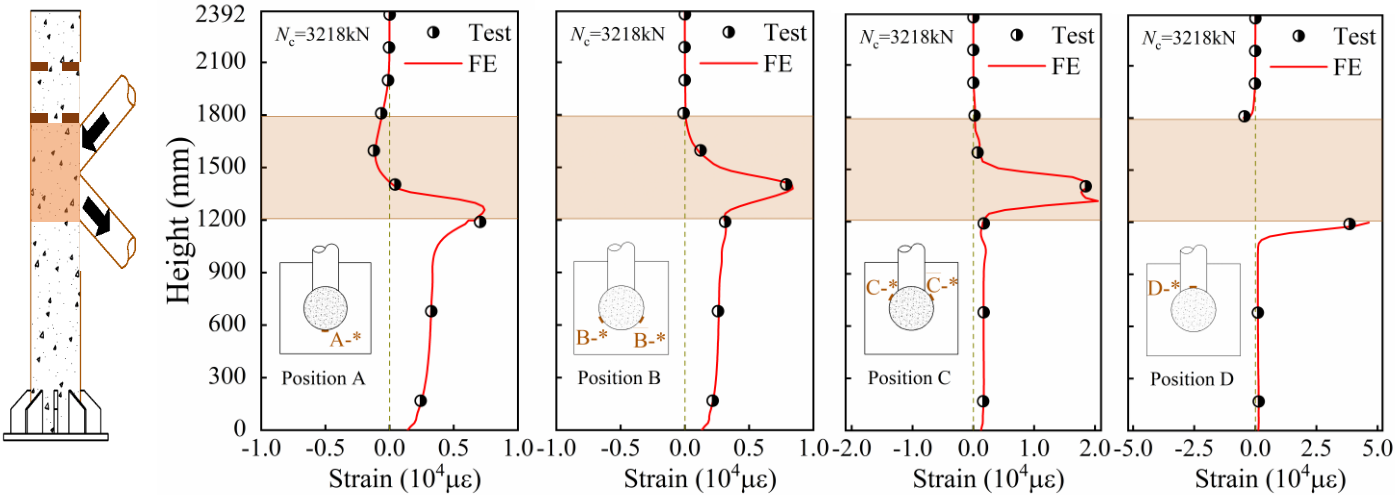

(c) A600-B1208-DP

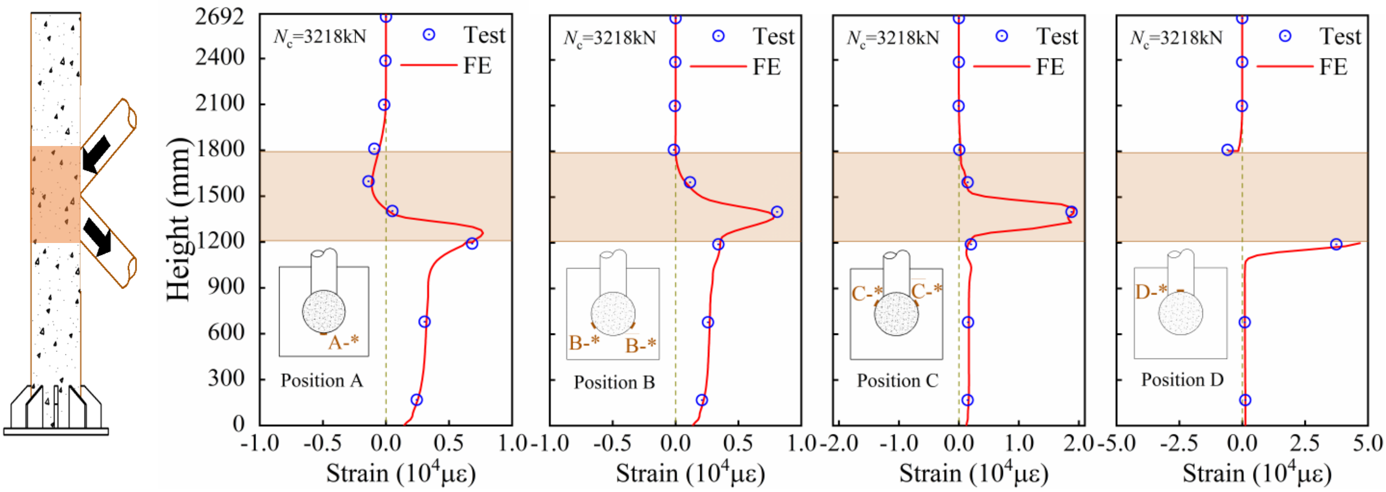

(d) A900-B1208-NP

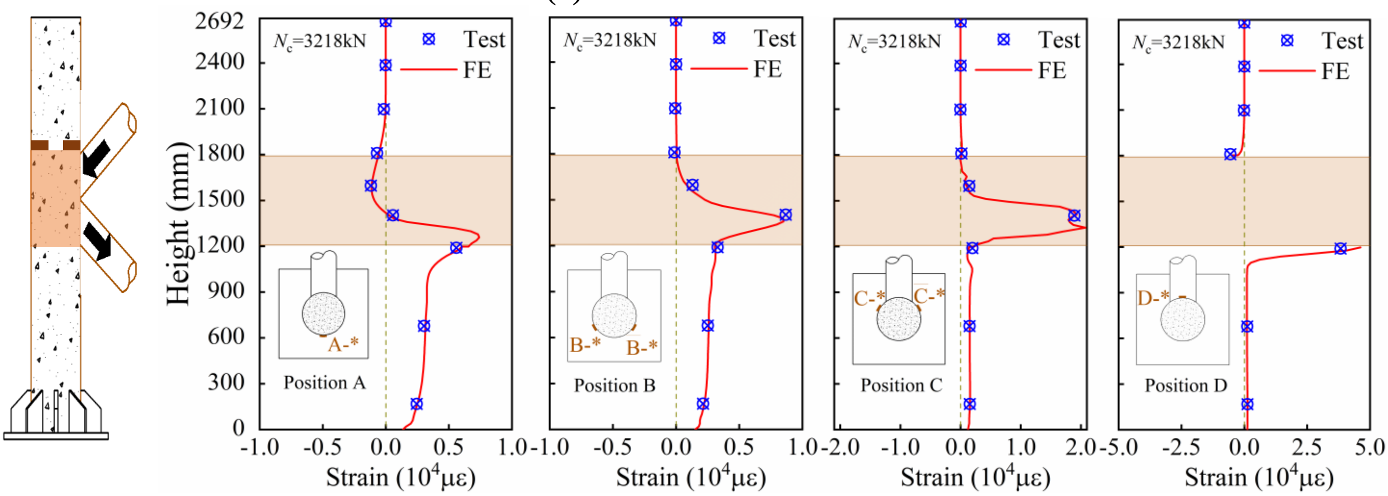

(e) A900-B1208-SP

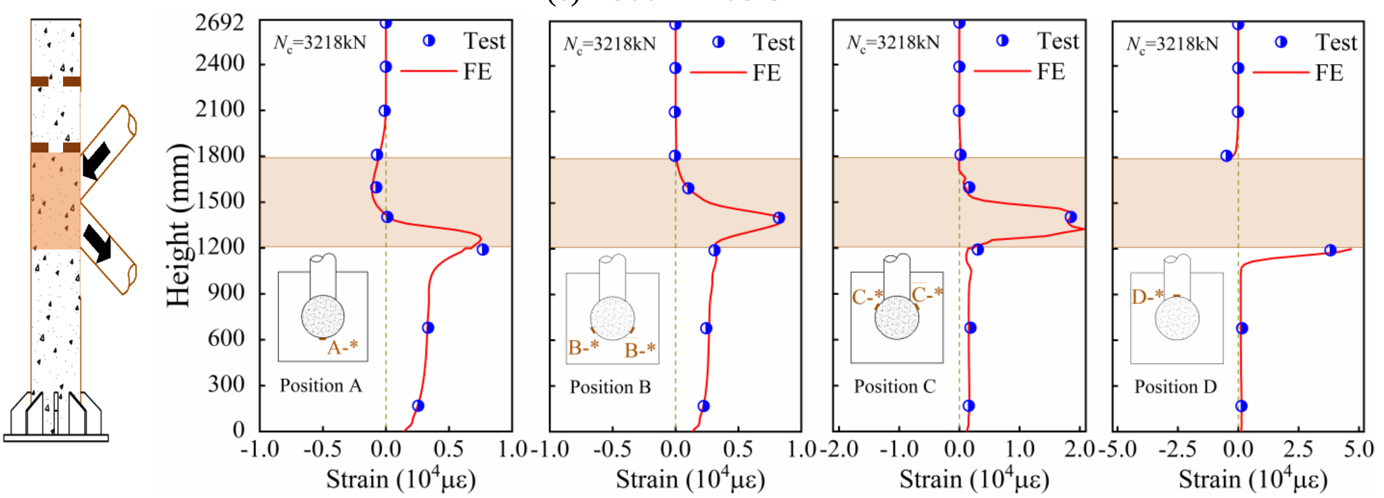

(f) A900-B1208-DP

Figure 7. Strain distributions of specimens

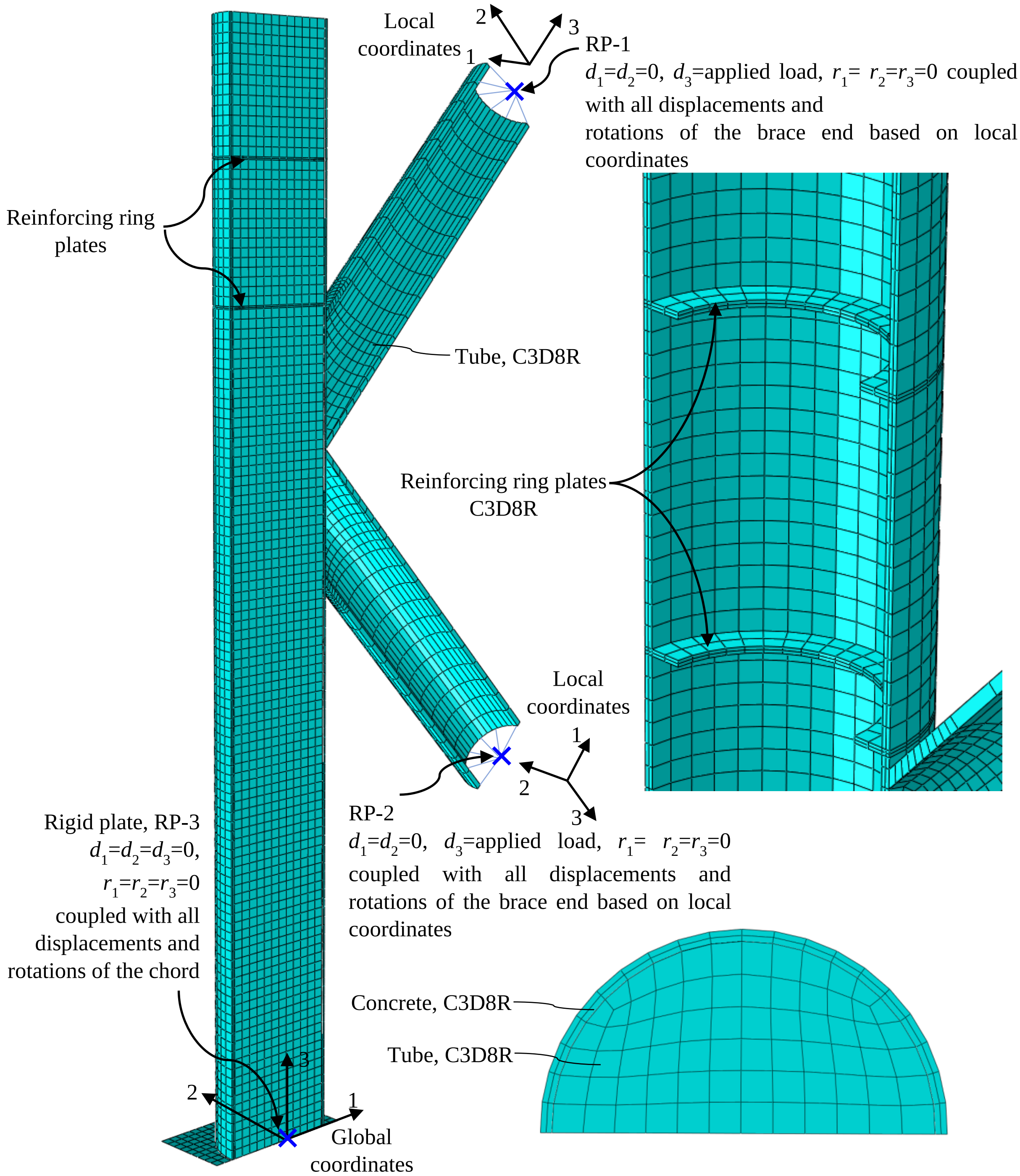

Figure 8. Schematic view of the FE model

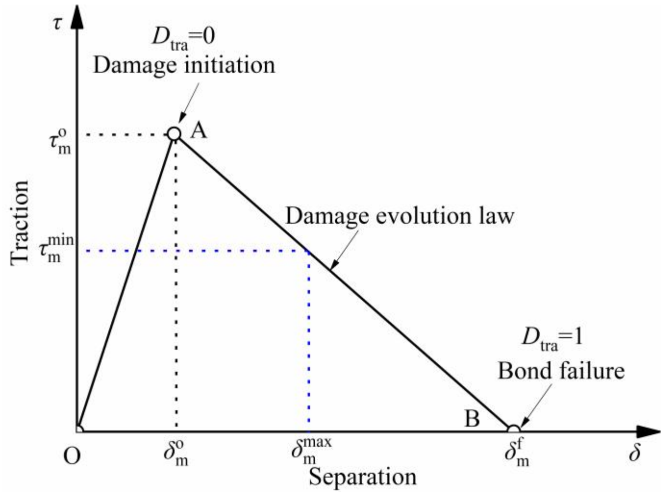

Figure 9. Traction-separation behaviour

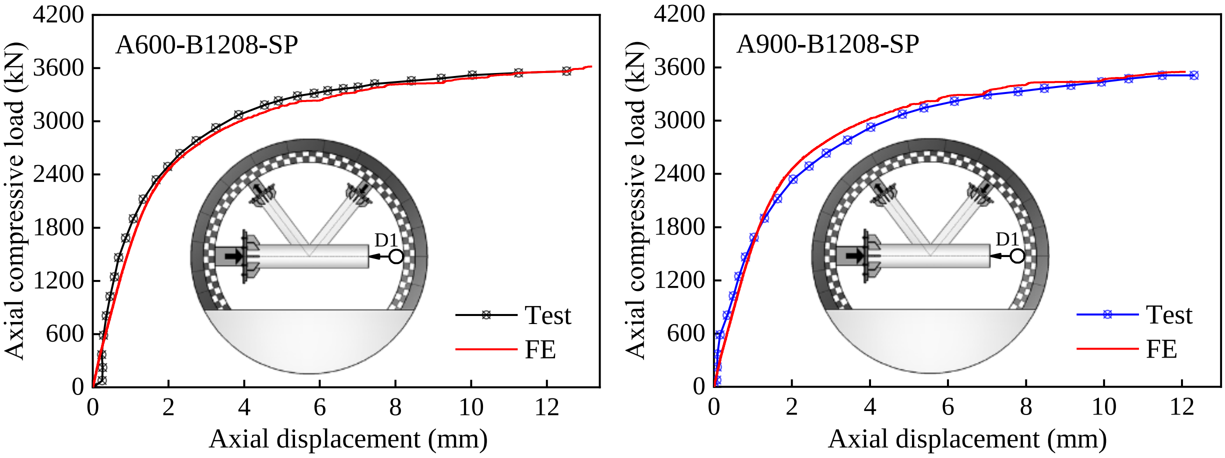

(a) A600-B1208-SP (b) A900-B1208-SP

Figure 10. Comparison of load-displacement curves between test and FE results

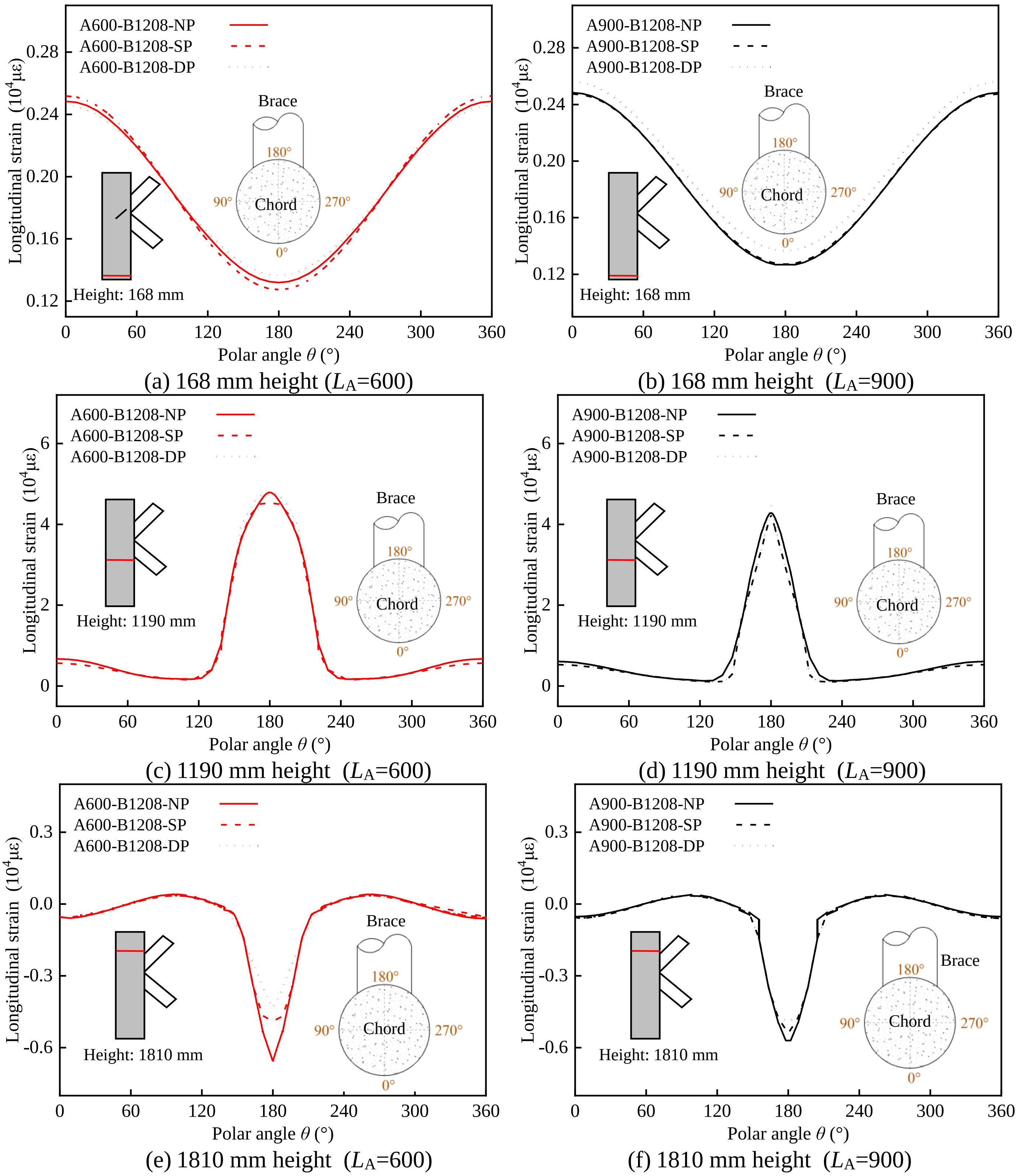

Figure 11. Longitudinal strain distribution along the circumferential direction of chord-wall

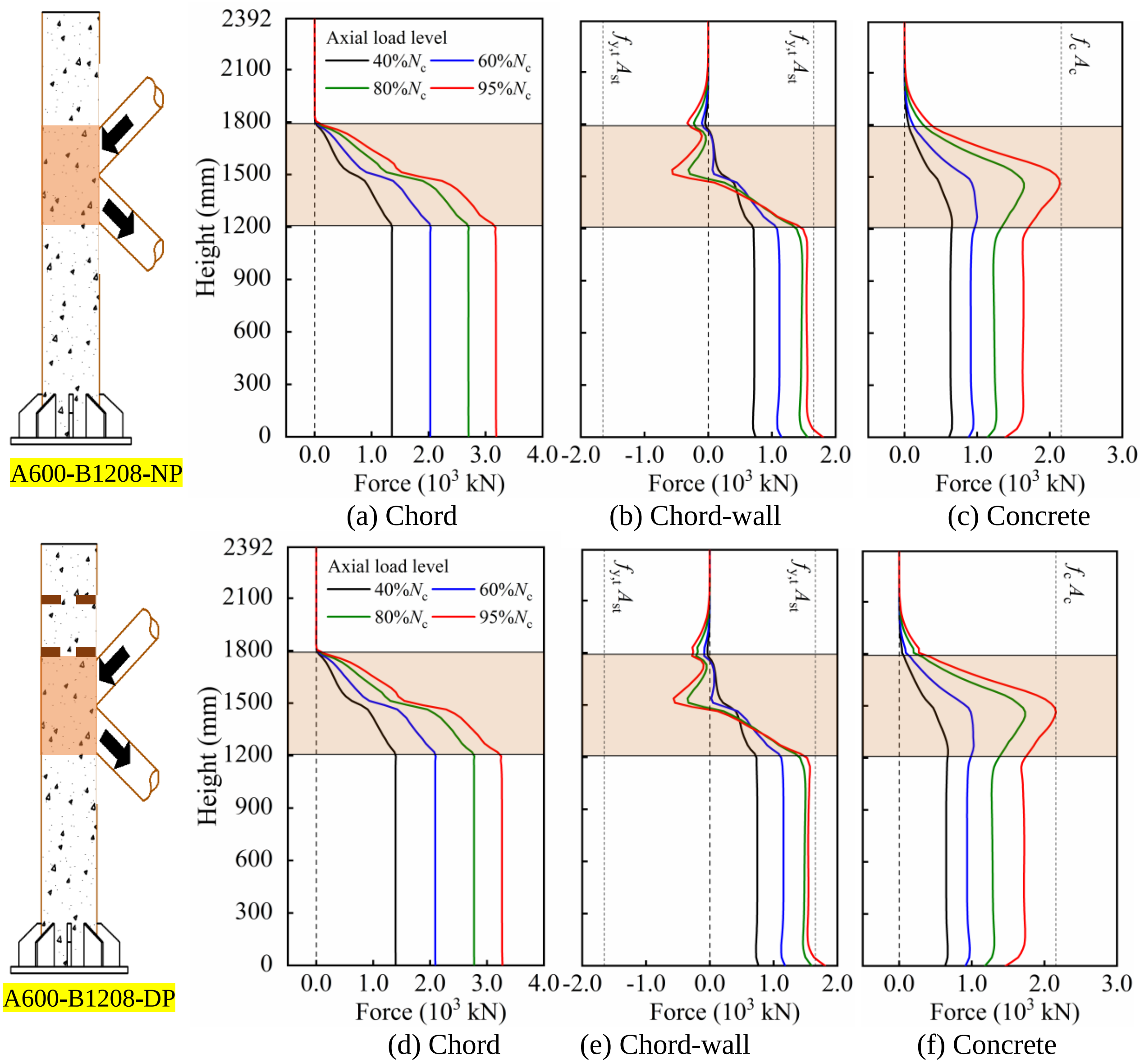

Figure 12. Force distribution of each component of the chord along with the height

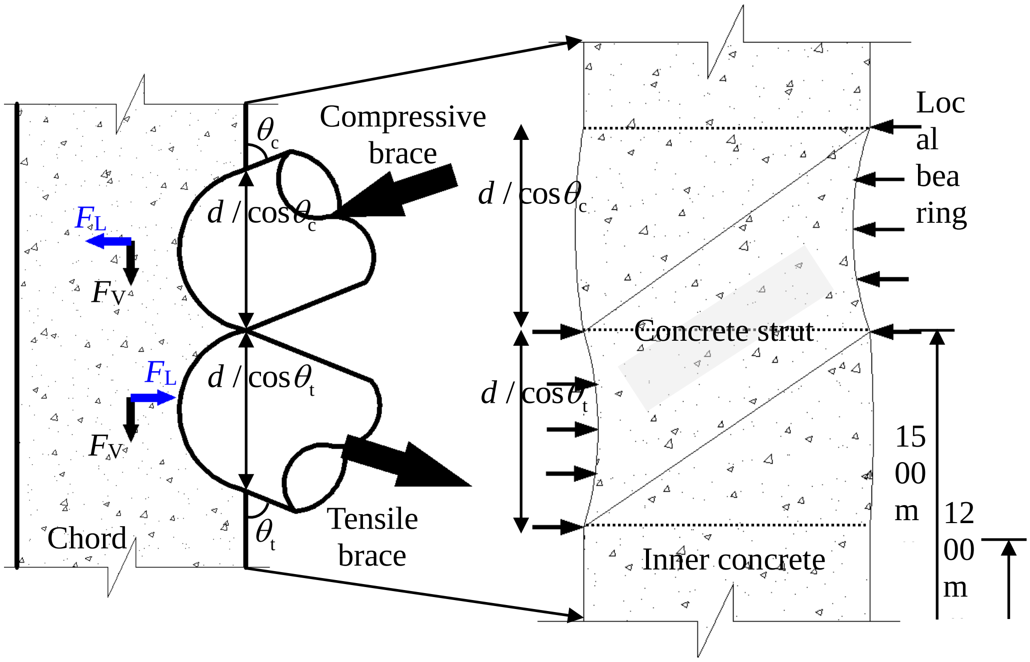

Figure 13. Lateral force components of the braces in the connecting region

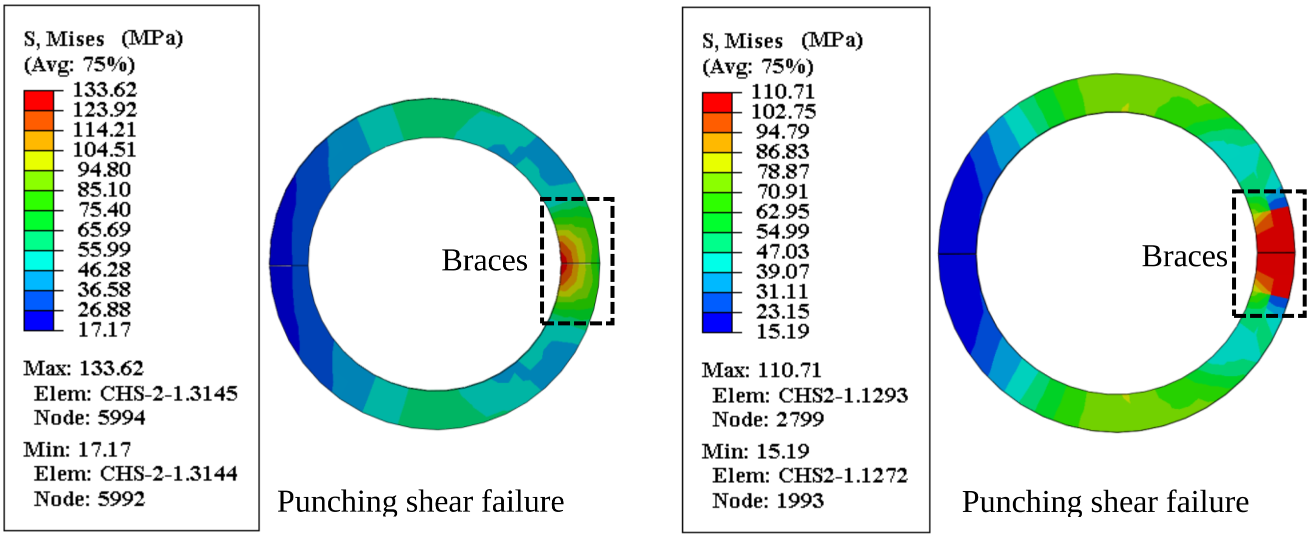

(a) A600-B1208-DP (b) D300T8A600B1208DP

Figure 14. Stress distribution of the reinforcing plate at the location of SP-1

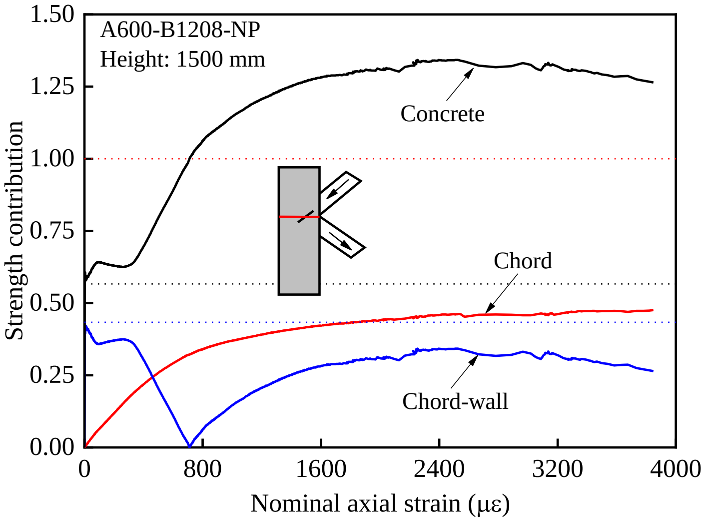

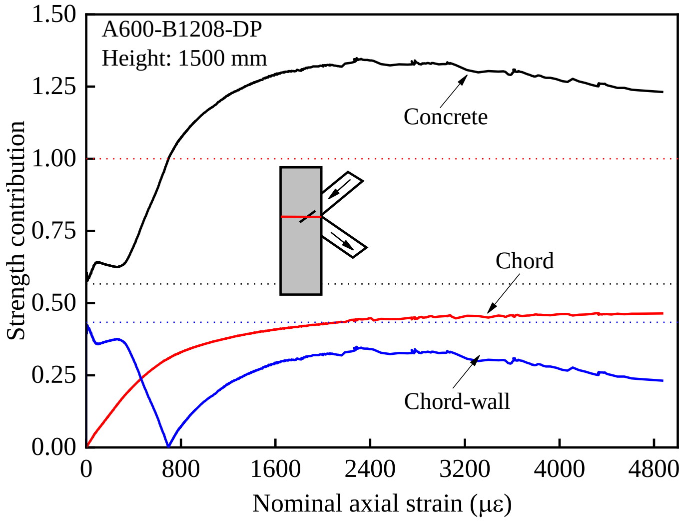

(a) 1500 mm height of A600-B1208-NP

(b) 1500 mm height of A600-B1208-DP

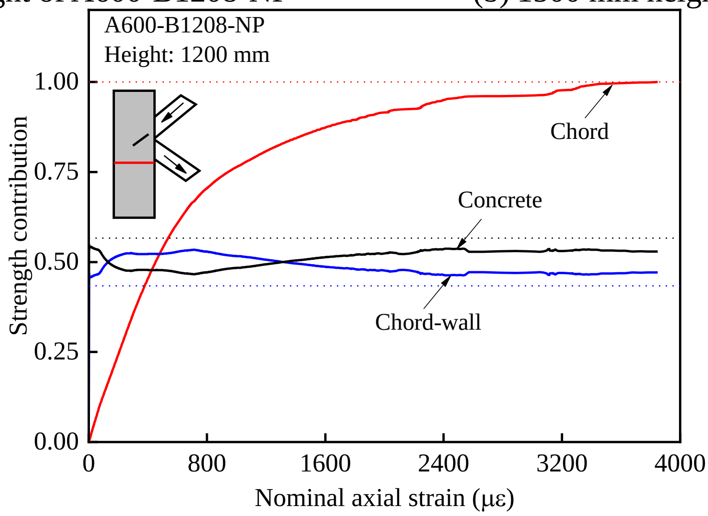

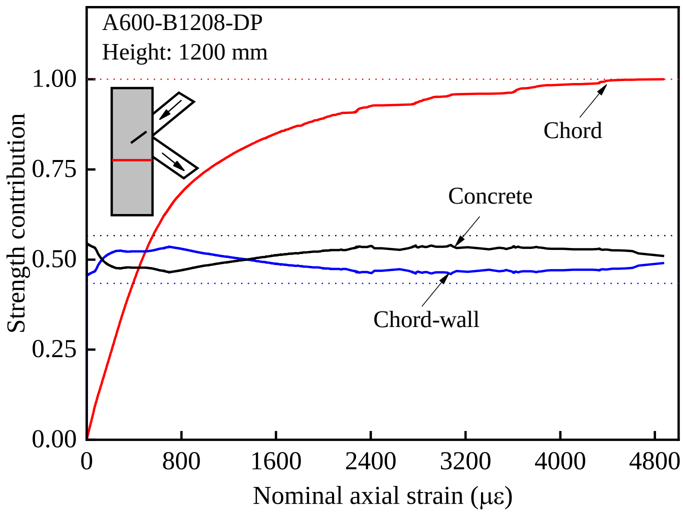

(c) 1200 mm height of A600-B1208-NP

(d) 1200 mm height of A600-B1208-

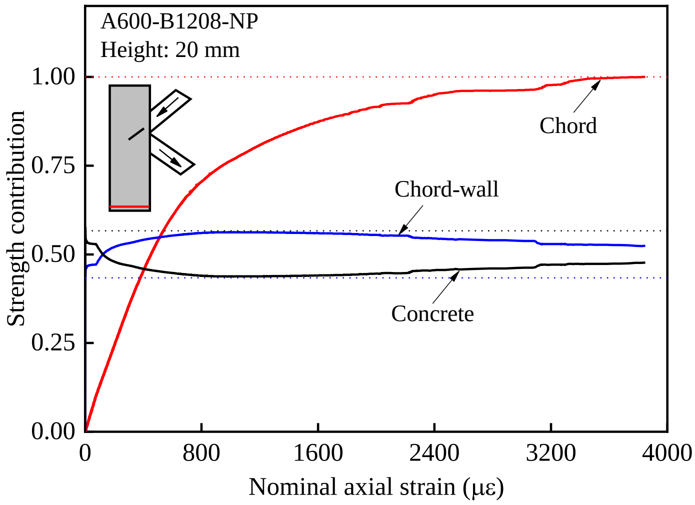

DP

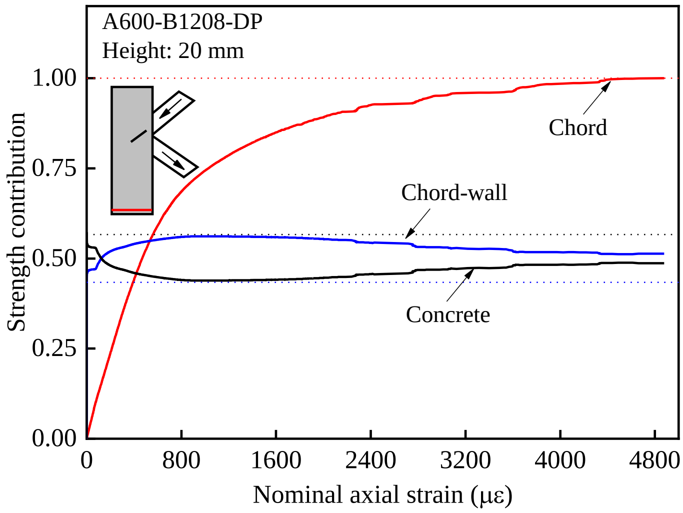

(e) 20 mm height of A600-B1208-NP (f) 20 mm height of A600-B1208-DP

Figure 15. Strength contributions of each component in the chord

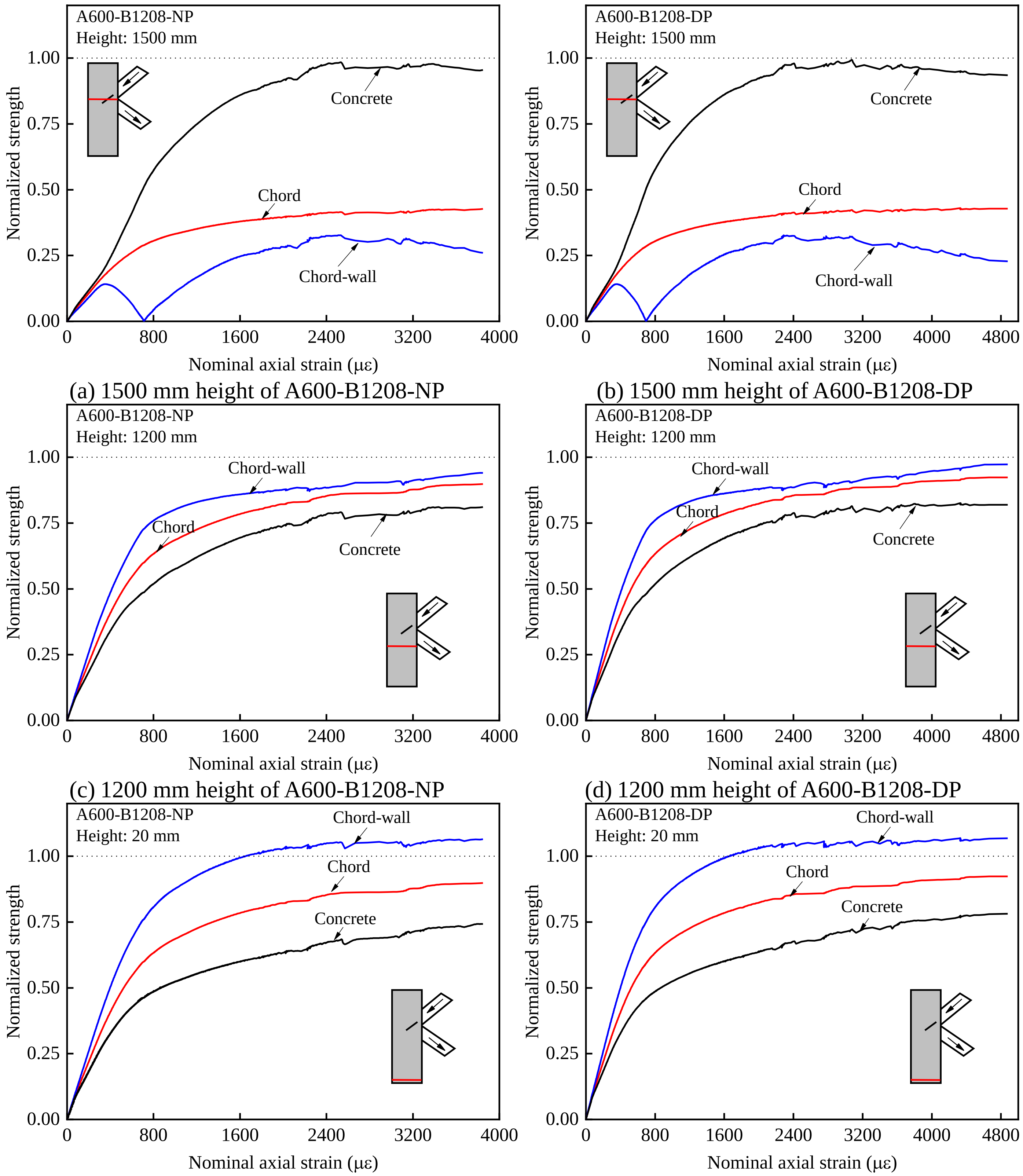

(a) 1500 mm height of A600-B1208-NP

(b) 1500 mm height of A600-B1208-DP

(c) 1200 mm height of A600-B1208-NP

(d) 1200 mm height of A600-B1208-DP

(e) 20 mm height of A600-B1208-NP

(f) 20 mm height of A600-B1208-DP

Figure 16. Strength utilization of each component in the chord

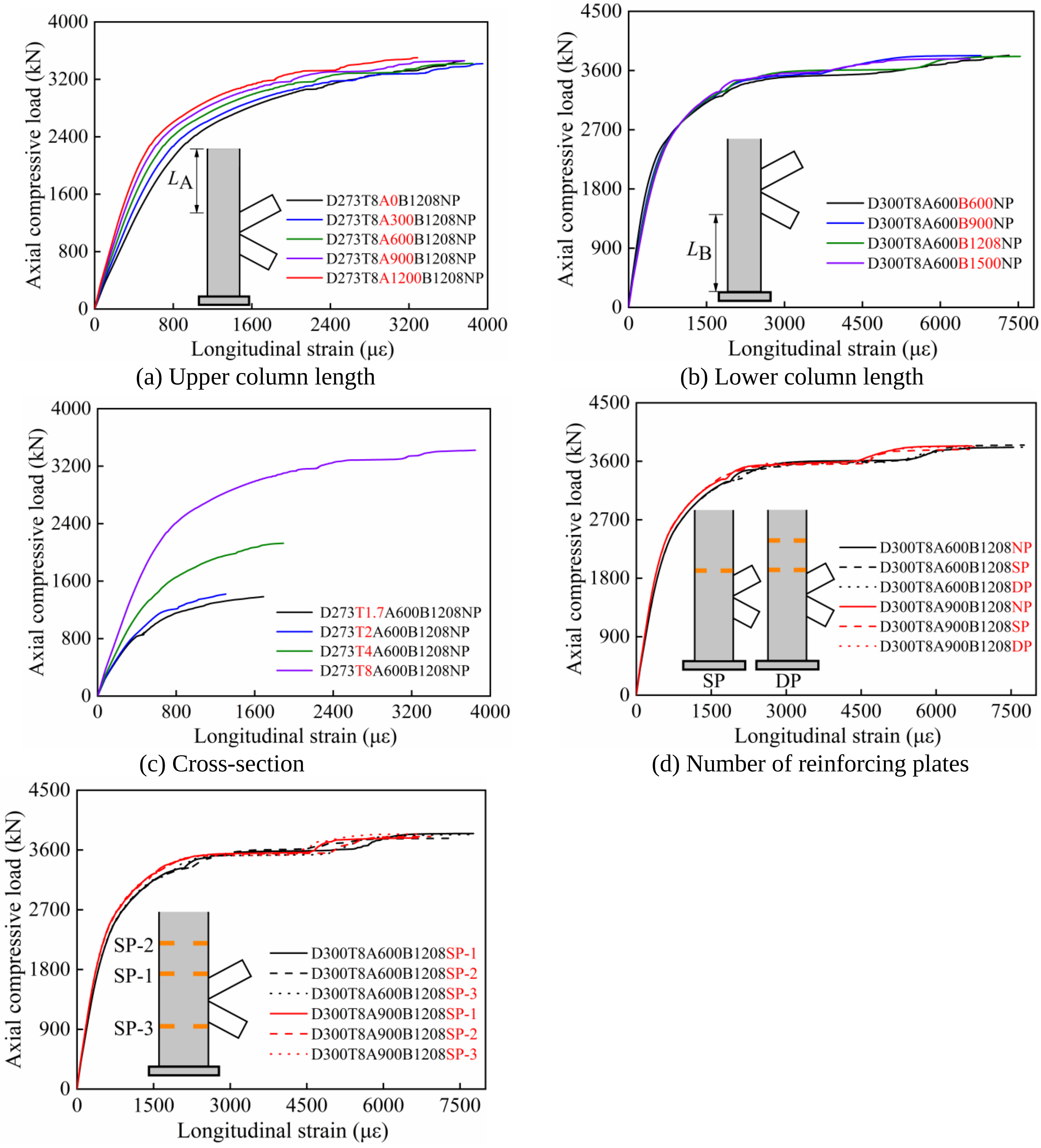

(a) Upper column length

(b) Lower column length

(c) Cross-section

(d) Number of reinforcing plates

(e) Position of reinforcing plates

Figure 17. Comparison of load-axial strain curves

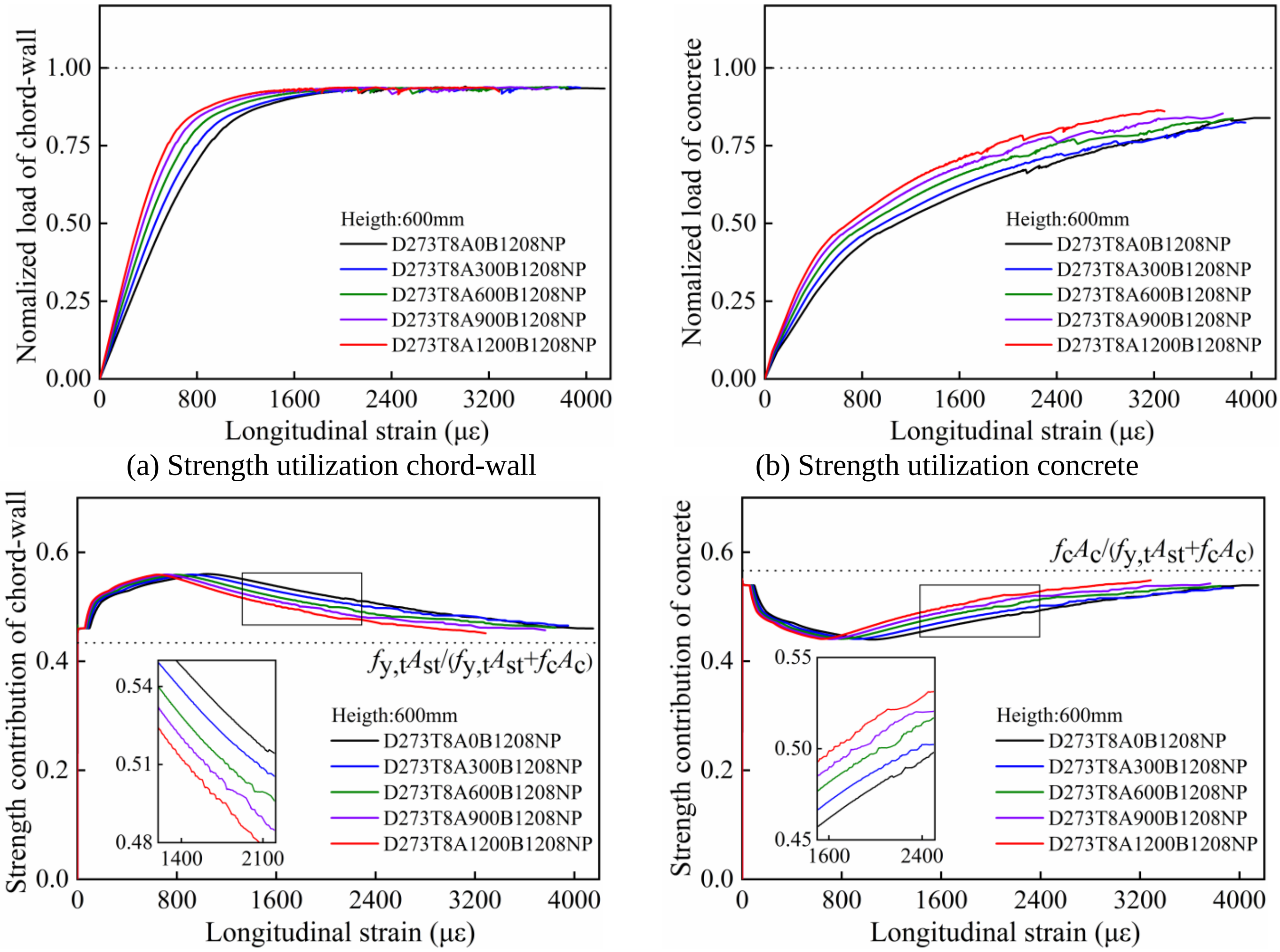

(a) Strength utilization chord-wall

(b) Strength utilization concrete

(c) Strength contribution chord-wall

(d) Strength contribution concrete

Figure 18. Strength utilization and contribution of each component: column length effect

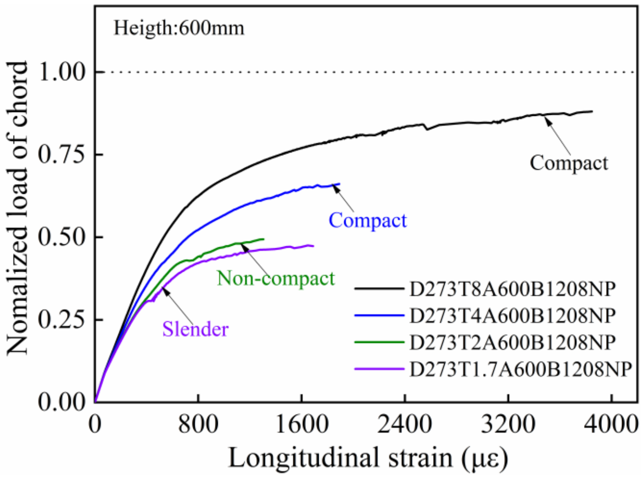

(a) Strength utilization chord

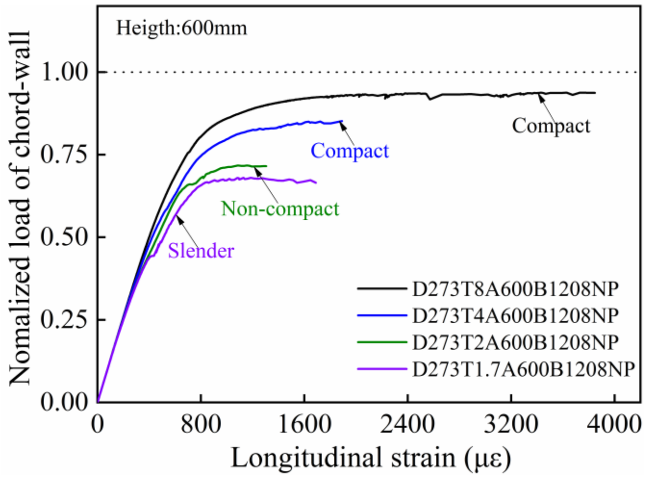

(b) Strength utilization chord-wall

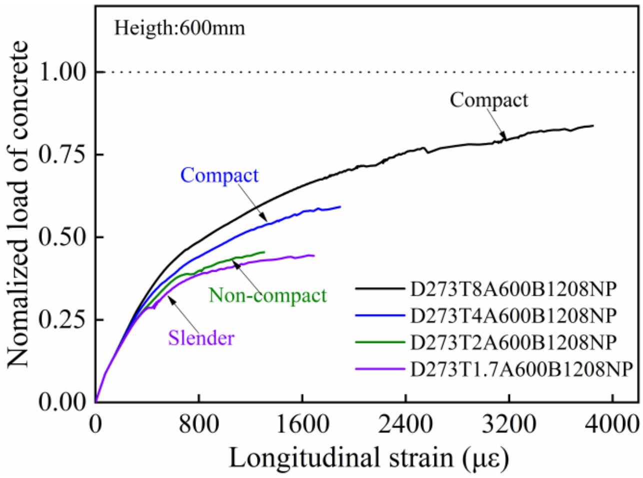

(c) Strength utilization of concrete

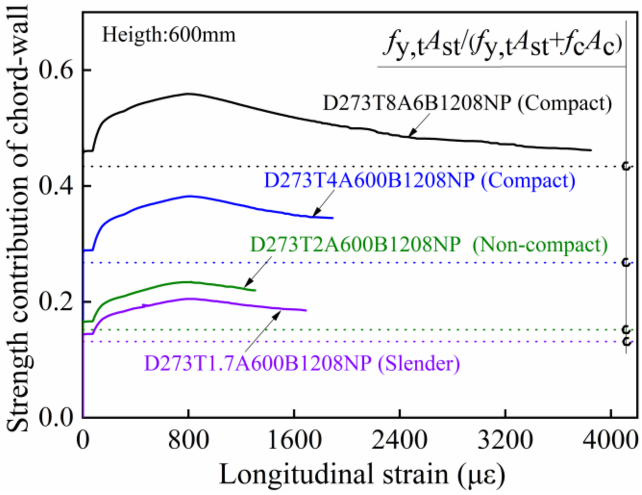

(d) Strength contribution of chord-wall

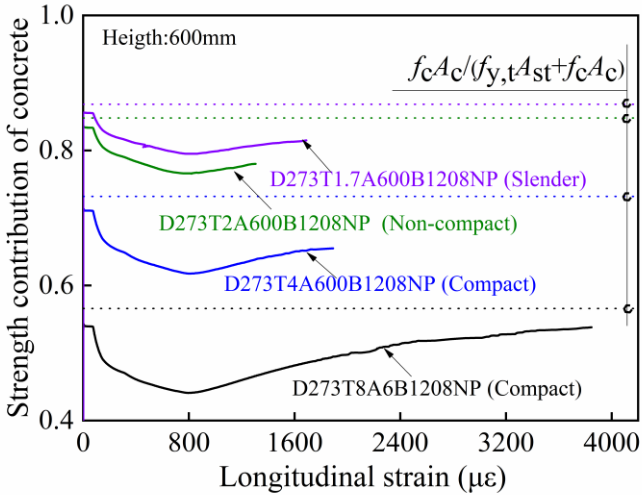

(e) Strength contribution of concrete

Figure 19. Strength utilization and contribution of each component: cross-section effect

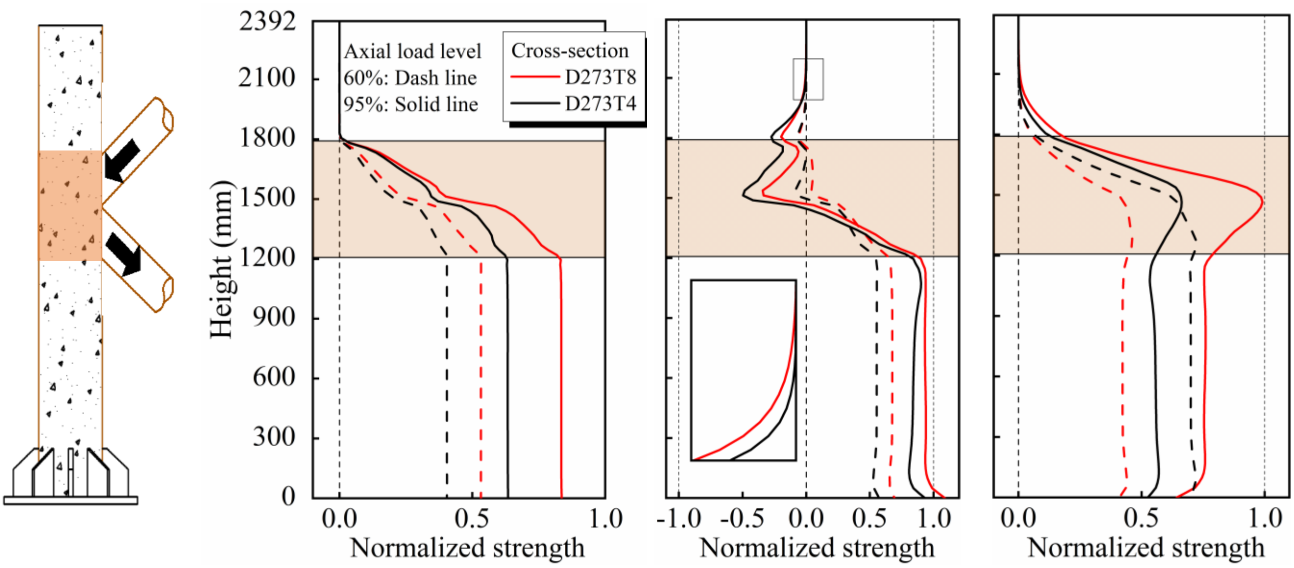

Figure 20. Force distributions of each component: cross-section effect

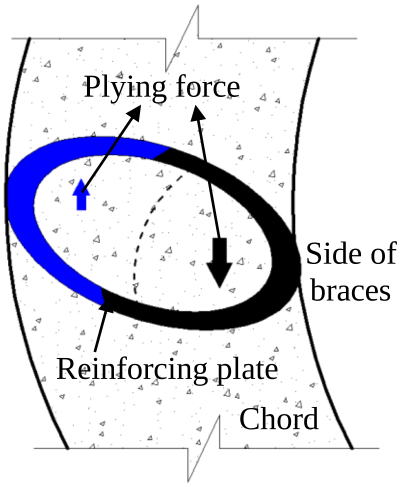

Figure 21. Plying force of reinforcing plate

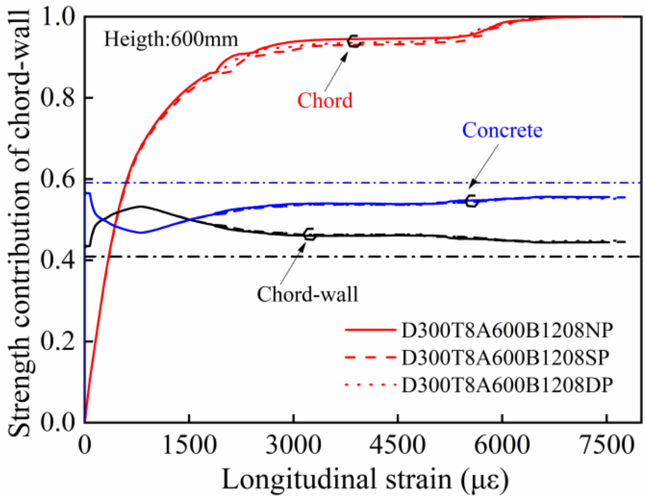

Figure 22. Strength contribution of each component: numbers of reinforce plate effect

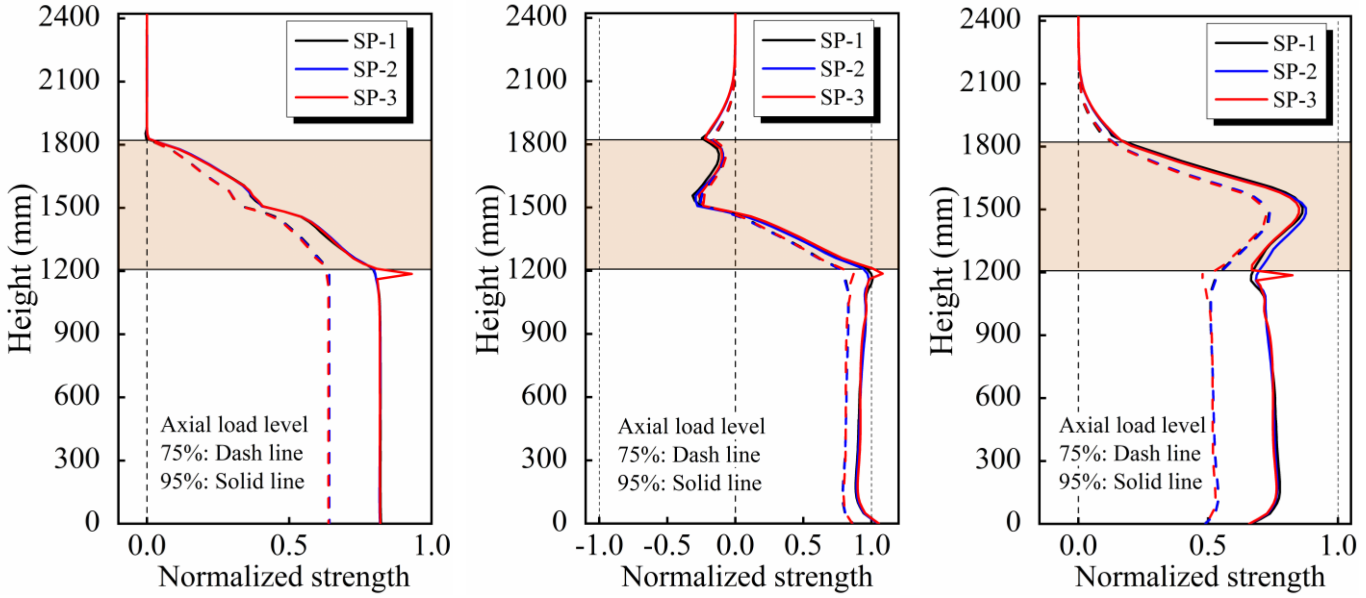

(a) Chord (b) Chord-wall (c) Concrete

Figure 23. Force distributions of each component: position of reinforcing plate effect

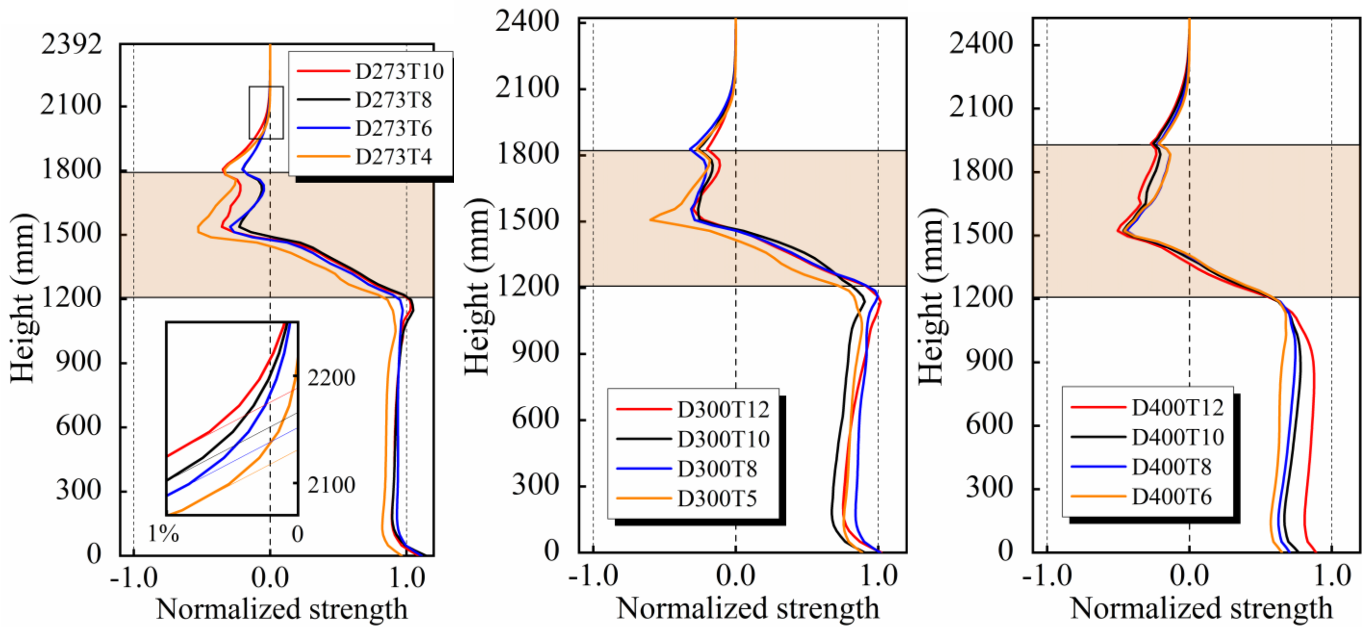

Figure 24. Load introduction length above the intersecting region of chord-wall

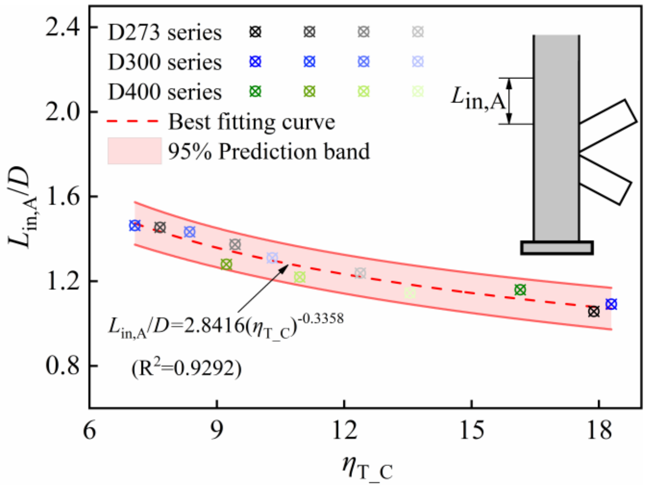

Figure 25. Predictions of load introduction length above the intersecting region

Table 1 Dimension details of specimens

Specimens	Nominal dimension of chord (mm)					Nominal dimension of brace (mm)			Punching shear strength $P_{u,test}$ (kN)	Axial compressive load $N_{c,test}$ (kN)
	L_A	L_B	L_C	D	T	l_b	d	t		
A600-B1208-NP	600	1208	584	273	8	1033	199	12	2374	3472
A600-B1208-SP	600	1208	584	273	8	1033	199	12	2437	3565
A600-B1208-DP	600	1208	584	273	8	1033	199	12	2365	3459
A900-B1208-NP	900	1208	584	273	8	1033	199	12	2334	3414
A900-B1208-SP	900	1208	584	273	8	1033	199	12	2401	3512
A900-B1208-DP	900	1208	584	273	8	1033	199	12	2450	3584

Note: L_A is the length above connecting region; L_B is the length below connecting region; L_C is the length of connecting region between chord and K-type braces; D is the diameter of chord wall; T is the thickness of chord wall; l_b is the length of brace; d is the diameter of the brace; t is the thickness of brace; $P_{u,test}$ is the punching shear strength of concrete-filled K CHS connection; $N_{c,test}$ is the axial compression load of chord when the specimen fails at punching shear fracture.

Table 2 Test results of tensile steel coupons

Item	Nominal thickness (mm)	E_s (GPa)	f_y (MPa)	f_u (MPa)
Chord wall	8.0	205.1	270.5	486.7
Brace	12.0	217.0	519.7	582.3
Reinforcing plate	6.0	203.2	276.2	432.8

Table 3 Comparison of experimental maximum compressive load and design predictions

Specimens	Punching shear strength (kN)			Axial compressive load (kN)			AISC design strength for CFST [15] $N_{u,AISC}$ (kN)	EC-4 design strength for CFST [16] $N_{u,EC4}$ (kN)	$\frac{P_{u,FE}}{P_{u,test}}$	$\frac{P_{u,test}}{P_u}$	$\frac{P_{u,FE}}{P_u}$	$\frac{N_{c,test}}{N_{u,AISC}}$	$\frac{N_{c,test}}{N_{u,EC4}}$
	Test $P_{u,test}$	FE $P_{u,FE}$	Prediction [11] P_u	Test $N_{c,test}$	FE $N_{c,FE}$	Prediction [11] N_c							
A600-B1208-NP	2374	2340	2440	3472	3423	3569	3655	4331	0.99	0.97	0.96	0.95	0.80
A600-B1208-SP	2437	2474	2400	3565	3618	3569	3655	4331	1.02	1.02	1.03	0.98	0.82
A600-B1208-DP	2365	2407	2440	3459	3521	3569	3655	4331	1.02	0.97	0.99	0.95	0.80
A900-B1208-NP	2334	2365	2440	3414	3460	3569	3655	4331	1.01	0.96	0.97	0.93	0.79
A900-B1208-SP	2401	2428	2440	3512	3551	3569	3655	4331	1.01	0.98	1.00	0.96	0.81
A900-B1208-DP	2450	2499	2440	3584	3655	3569	3655	4331	1.02	1.00	1.02	0.98	0.83
								Mean	1.01	0.98	0.99	0.96	0.81
								COV	0.012	0.023	0.029	0.019	0.019